Framework for Analytical Solutions of the Navier-Stokes Equations for Hyperbolic Boundary Value Problems in the Aerodynamic Near-Field

Steven A. E. Miller*
Former DARPA Director's Fellow for Hypersonics

A framework to create new specific analytical solutions of the equations of motion for hyperbolic boundary value problems is presented. The method relies on a closed-form integral equation for mass density, involving a term that combines sources, geometry, ambient values, and radiation. Products of the density integral result in new more complicated solutions. The density field is used to recover the field variables in the near-field through far-field relative to the aerodynamic body. The aerodynamic body is modeled as a product and combination of generalized functions. Thus, resultant analytical solutions are also a combination of generalized functions. Derivations of time-dependent analytical solutions and example predictions are presented in one and two spacial domains. Cases examined for Euler equations include moving shock waves, oblique shock waves, Prandtl-Meyer expansions, and fields from more complicated bodies. A discussion of limitations and future directions of the methodology is included. The methodology, in a more complicated form, is used primarily for hypersonic sonic boom prediction.

I. Introduction

The equations of motion are solved for specific analytical solutions of hyperbolic boundary value problems and are dependent on space and time. Specific closed-form analytical solutions for hyperbolic flow-fields, which are those that are entirely supersonic everywhere, are proposed for simple through complicated cases. Most importantly, a framework that theoreticians can follow can be used to construct new analytical solutions is presented. New solutions are created from simpler solutions using a newly proposed product algorithm. Closed-form solutions are for mass density, which is used to construct other field-variables using traditional theory. The resultant solution consists of the full compressible field-variables for density, velocity, pressure, and temperature. This integral method and product of solutions algorithm is programmed into a new computer program called the Integral Method Program (IMP), which creates solution files consisting of generalized functions instead of numerical values. In this paper, the background, theory, predictions, and framework are presented. This research is the basis for a new kind of prediction algorithm being developed to predict

*Research conducted while DARPA Director's Fellow for Hypersonics and leader of the Theoretical Fluid Dynamics and Turbulence Group. saemiller@gmail.com and https://saemiller.com

complete flow-fields around supersonic and hypersonic aerodynamic bodies.

A. Motivation

There are multiple motivational factors for the present research. The first is to create new analytical methods to predict near-field aerodynamics around slender hypersonic flight-vehicles. This leads to enhanced design, signature detection, and prediction capability of sonic boom. Presently, there are four main methods to ascertain the near-field pressure suitable for sonic boom prediction from slender hypersonic flight-vehicles. Experiments are very successful; however, it is very difficult or next to impossible to perfectly match wind tunnel tests [1–3] with flight-tests. Computational Fluid Dynamics (CFD) can successfully predict the pressure near-field [4–7], however, CFD is very computationally expensive, not suited for fast prediction studies, cannot directly predict the far-field, and requires expert users with decades of experience. Relative to analytical methods, CFD generally cannot directly connect first principles equations of motion to the physics of the flow-field as only numerical results are present. Two major analytical approaches have been previously developed. The original method of Whitham [8, 9] and Carlson [10] (lift effects) rely on linearized aerodynamic theory and use the famous F-function, which provides a near-field pressure via integration. Unfortunately, these theories are limited to slender vehicles between Mach numbers 1.2 to 3.0 (see Hayes [11], Hayes and Runyan [12]). For bluff body hypersonic flows, an instantaneous impulse method was developed by Seebass [13] and Tiegerman [14]. Their methods are valid for bluff bodies with a cylindrical fuselage of infinite length that generates no lift. Lift accounts for over 40% [15] of the boom overpressure at moderate supersonic speeds. Clearly, there is a need for a new hypersonic near-field pressure based sonic boom prediction scheme that also accounts for lift from slender bodies. The present method does not use linearized theory due to strong flow nonlinearities. The method is compatible with existing sonic boom propagation codes (e.g. PCBOOM [16]).

Another major motivational factor was presented by the NASA 2030 CFD Vision [17]. The vision was crafted by a consortium of industrial, government, and academic entities, delineates enhancements in grid generation, CFD solvers, post-processing, and ancillary technologies. Contemporary research is predominantly centered on machine learning [18] and high-performance computing [19] for CFD. An integral aspect of the NASA 2030 vision is bench-marking and augmentation of CFD codes, aiming to validate CFD with experiments. The present method can serve as a benchmark for emerging HPC and combined CFD machine learning codes.

The Clay Mathematics Foundation has posed several challenge problems to the global mathematical community. Among these, the problem concerning the Navier-Stokes equations, specifically focusing on the proofs of breakdown or the existence and smoothness of initially smooth, incompressible flow-fields, is of interest [20]. The institute is interested in proofs rather than prediction methodologies. Although the incompressible assumption renders these efforts practically inapplicable as all fluids exhibit some degree of compressibility (e.g. acoustic waves). The present methodology seeks to strengthen the understanding of fluid dynamics, aligning with the core objective of the Clay Mathematics

Navier-Stokes challenge. Contrary to this theoretical pursuit, the current approach is dedicated to prediction and the derivation of new specific solutions for steady hyperbolic flow-fields.

The present research aims to develop an ultra-fast prediction framework for the Euler [21, 22] and Navier-Stokes equations [23, 24], focusing on generating specific analytical solutions in entirely supersonic flow-fields. The next subsections illustrate previous prediction methods that the present research draws upon.

1. Near-Field Prediction for Sonic Boom and Whitham's F-Function

Two major analytical approaches have been previously developed. The original method of Whitham [8, 9] and Carlson [10, 25] (lift effects) rely on linearized aerodynamic theory and use the famous F-function, which provides a near-field pressure via integration. Unfortunately, these theories are limited to slender vehicles at Mach numbers of 1.2 to 3.0 (see Hayes [26], Hayes et al. [27]). For bluff body hypersonic flows, an instantaneous impulse method was developed by Seebass [13], Tiegerman [14], and Cramer [28, 29]. Their methods are valid for a bluff body with a cylindrical fuselage of infinite length that generates no lift. Their models account for the body volume only, which easily contributes to over 40% [15] of the sonic boom overpressure at moderate supersonic speeds. Example predictions are shown in Morris et al. [30] and Hunton [31], where predictions depart from measurement at high-speeds. There is a need for a new hypersonic near-field pressure based sonic boom prediction scheme that also accounts for lift from slender bodies. New methods must be nonlinear to account for the strong nonlinearities present in the near-field.

The F-function [8–10, 25] relies on linearized supersonic theory and corrections for lift. Typically, this pressure time history is propagated through the atmosphere with sonic boom propagation solvers. The theory leads to the basic equation for static pressure about the atmospheric pressure

$$\Delta p(x-\beta_{\mathrm{P}} r, r) = \frac{p_\infty \gamma M^2 F(x-\beta_{\mathrm{P}} r)}{(2\beta_{\mathrm{P}} r)^{1/2}}, \tag{1}$$

where M is the Mach number, p is the pressure, p_∞ is the ambient pressure, r is the radial location, x is the streamwise location, β_{P} is the Prandtl-Glauert factor, and γ is the ratio of specific heats. The F-function is

$$F(x) = \frac{1}{2\pi} \int_0^x \frac{A''(\xi)}{(x-\xi)^{1/2}} d\xi, \tag{2}$$

where A is the local cross-sectional area. A is modified by Cramer [28] as

$$A_L(x,\theta) = \frac{\beta_p}{\rho u_\infty^2} \int_0^x L(xi,\phi) dxi, \tag{3}$$

to account for lift. Here, A_L is modified area, L is the component of lift per unit length, u_∞ is the ambient velocity, ξ is an axial variable of integration, and ϕ is the azimuthal coordinate. Even though the F-function accounts for lift and is designed for slender bodies, the disagreement at hypersonic speeds is unacceptable. In the present approach, the F-function is similar to the thickness or displacement term and the lift-correction corresponds to the loading term, which will be shown.

2. Oseen's Approach

Explicit formulas for hydrodynamic potentials of Lorentz (1896) and Oseen [32], further utilized by Leray [33] were used to create weak solutions of the Navier-Stokes equations. These are sometimes called evolutionary Stokes' equations and are then applied to Navier-Stokes equations. Oseen [32] proposed a tensor O_ν (now called Oseen's tensor) such that the Stokes' equations are

$$\partial_t \boldsymbol{u} = -\nabla \boldsymbol{p} + \nu \Delta \boldsymbol{u} + \boldsymbol{F}, \tag{4}$$

with the D'Alembert condition ($\nabla \cdot \boldsymbol{u} = 0$). Velocity $\boldsymbol{u}(\boldsymbol{x}, t)$ has the solution for positive t as

$$\begin{aligned} \boldsymbol{u}(\boldsymbol{x},t) = &\int W_\nu(\boldsymbol{x}-\boldsymbol{y},t)\boldsymbol{u}(\boldsymbol{y},0)dy \\ &+ \int_0^t \int O_\nu(\boldsymbol{x}-\boldsymbol{y},t-\tau) \\ &\times \left(\boldsymbol{f}(\boldsymbol{y},\tau) - \sum_{i=1}^{3} u_i(\boldsymbol{y},\tau)\partial_i \boldsymbol{u}(\boldsymbol{y},\tau) \right) d\tau d\boldsymbol{y}. \end{aligned} \tag{5}$$

Here, $\boldsymbol{F}$ and f are force, p is static pressure, t is time, $\boldsymbol{u}$ is the velocity vector, $\boldsymbol{x}$ is the location of prediction or observer location, $\boldsymbol{y}$ is source location and is a spatial location, τ is source time, and ν is dynamic viscosity. Bold symbols denote vectors. W_ν is the heat kernel of the associated heat equation, $\partial_t G = \nu \Delta G$. The solution is closed and can be found for very small time intervals when the initial condition and force are regular and localized. Note that this system is incompressible, but shows that solutions can be written in an integral form for velocity.

3. Lighthill's Acoustic Analogy

Lighthill [34, 35] created the acoustic analogy in a series of three papers. An acoustic analogy is a rearrangement of the governing equations into a linear wave equation that is equated with equivalent sources. Lighthill [34] used a Green's function and convolution integral with an equivalent source to predict the density fluctuations from turbulent fields. In the present paper, density is sought in the form of an integral equation. Equation 15 of Lighthill [34] is

$$\rho - \rho_\infty = \frac{1}{4\pi c_\infty^2} \frac{\partial^2}{\partial y_i \partial y_j} \int T_{ij} \left(\mathbf{y}, t - \frac{|\mathbf{x} - \mathbf{y}|}{c_\infty} \right) \frac{\mathrm{d}\mathbf{y}}{|\mathbf{x} - \mathbf{y}|}, \tag{6}$$

where c_∞ is the ambient speed of sound, T_{ij} is the Lighthill stress tensor, and ρ is the density.

The theory represented the birth of contemporary aeroacoustics. Acoustic analogies are linear theories, and only recently has one been modified to account for nonlinear propagation through replacement of the propagation operator with a numerical solution of the generalized Burgers' equation (see Miller [36]). Though Miller's approach is fairly limited to specific situations, and cannot account for sources that produce shock waves directly.

Lighthill [34] wrote the density as a closed-form equation involving integration over space-time (Eqn. 6). One important point of Lighthill's [34] theory is that to solve the equation, one must know the solution of the Navier-Stokes equations. After all, Eqn. 6 is a rearrangement of the continuity and momentum equation. That is specifically, the source term T_{ij} contains unknown field-variables beyond typical initial and boundary conditions. Nonetheless, Lighthill's approach is useful for linear acoustics and not the present nonlinear problem.

B. Overview of the Paper

The remaining portion of this paper is laid out as follows. First, the analytical theory is developed and its implementation is described. Then, a number of predictions are presented that recover classical analytical solutions of time dependent one- and two-dimensional flow-fields. The limitations of the methodology are discussed and conclusions are drawn.

II. Theory

The basis of the present approach are the Navier-Stokes equations [23, 24, 37]. The conservation of mass or continuity equation is

$$\frac{\partial \rho}{\partial t} + \frac{\partial \rho u_j}{\partial x_j} = 0, \tag{7}$$

where t is time, $\boldsymbol{u}$ is the velocity vector, $\boldsymbol{x}$ is the spatial coordinate, and ρ is mass-density. Einstein or index notation is used. The conservation of momentum equation is

$$\frac{\partial \rho u_i}{\partial t} + \frac{\partial \rho u_i u_j}{\partial x_j} = \frac{\partial \tau_{ij}}{\partial x_j}, \tag{8}$$

where p is pressure and δ_{ij} is the Kronecker delta function. The tensor τ_{ij} is

$$\tau_{ij} = -p\delta_{ij} + \mu\left(\frac{\partial u_i}{\partial x_j} + \frac{\partial u_j}{\partial x_i}\right) + \zeta\delta_{ij}\frac{\partial u_k}{\partial x_k}, \tag{9}$$

where μ is the first coefficient of viscosity and ζ is the second coefficient of viscosity. The conservation of energy equation is

$$\frac{\partial \rho e_o}{\partial t} + \frac{\partial \rho u_j e_o}{\partial x_j} = -\frac{\partial q_j}{\partial x_j} + \frac{\partial u_i \tau_{ij}}{\partial x_j}, \tag{10}$$

where e is energy. Total energy e_o is

$$e_o = e + \frac{u_k u_k}{2}. \tag{11}$$

Heat transfer is

$$q_j = -c_p \frac{\mu}{P_r}\frac{\partial T}{\partial x_j}, \tag{12}$$

where $P_r = c_p \mu \lambda^{-1}$, c_p is the coefficient of specific heat at constant pressure, and λ is thermo-conductivity. Ratio of specific heat is $\gamma = c_p c_v^{-1}$, where c_v is coefficient of specific heat at constant volume. The system is closed by the ideal gas law

$$p = \rho R T, \tag{13}$$

where R is the gas constant T is static temperature.

A. Generalized Equations of Motion

The flow-field is governed by the Navier-Stokes equations (Eqns. 7 and 8), energy Eqn. 10, and gas law Eqn. 13. The source field (generated by an aerodynamic body) must be predicted with a nonlinear equation without making a linearization assumption. Density, ρ, is directly sought with the continuity and momentum equations. To accomplish this goal, define a sigma surface (see Ffowcs Williams and Hawkings [38] and Miller [39]), S. The surface is defined by a function f with $\delta(f) = 0$ and is a closed surface. The generalized function, δ, is the Dirac delta function (see [40][41]). The function has the property of $f \leq 0$ inside the surface, and $f > 0$ outside the surface. In the present formulation,

surface integrals over S are replaced by volume integrals using the generalized function $\delta(f)\left\{(\partial f/\partial x_j)^2\right\}^{\frac{1}{2}}$. The system of equations using this notation is shown in Fig. 1, where the entire fluid volume is denoted as V, which is separated into two regions, Region 1 and Region 2. In this application, the volume V is infinite, and Region 2 is finite, while Region 1 is infinite. The surface S is the body surface. The function f represents the aerodynamic body's shape. Velocity vector, $\boldsymbol{v}$, is the body velocity.

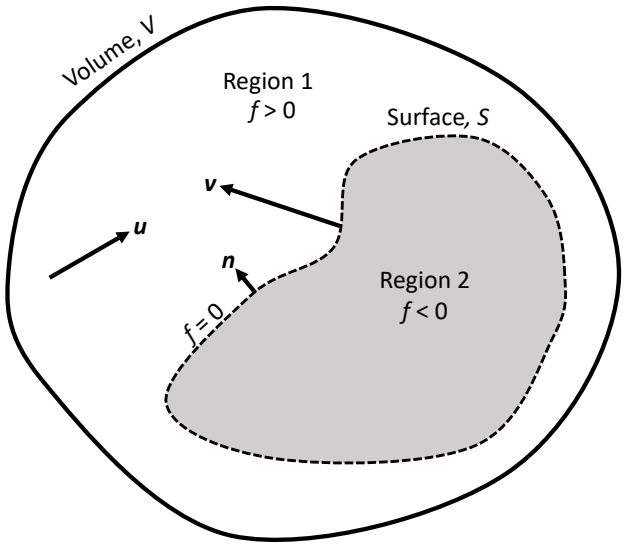

Fig. 1 Formulation of system of equations.

Using Eqns. 7 and 8 and noting that $n_i\left\{(\partial f/\partial x_j)^2\right\}^{\frac{1}{2}}$ is equal to $\partial f/\partial x_i$ (see Gelfand and Shilov [42]), the generalized continuity equation can be written as

$$\frac{\partial \overline{\rho}}{\partial t} + \frac{\partial \overline{\rho u}_i}{\partial x_i} = \rho v_i \delta(f) \frac{\partial f}{\partial x_i} \tag{14}$$

and momentum equation as

$$\frac{\partial \overline{\rho u}_i}{\partial t} + \frac{\partial}{\partial x_j}\left(\overline{\rho u_i u}_j + \overline{\tau}_{ij}\right) = \tau_{ij}\delta(f)\frac{\partial f}{\partial x_j}. \tag{15}$$

Generalized variables are denoted with an overbar. For linear solutions, it is possible to use the approach of the acoustic analogy discussed earlier. This resulted in the famous acoustic analogy of Ffowcs Williams and Hawkings [38]. However, the propagation term would be a linear wave equation. Here, the problem is cast as a nonlinear propagator.

Examine the equivalent source terms of Lighthill [34], Ffowcs Williams and Hawkings [38], and Miller [36]. The

Lighthill stress tensor is introduced in Eqn. 1 of Lighthill [34] and is

$$T_{ij,\,\text{Lighthill}} = \rho u_i u_j + p_{ij} - c_\infty^2 \rho \delta_{ij}. \tag{16}$$

Here, p_{ij} is the notation used by Lighthill [34, 35] as the compression stress term involving static pressure. Ffowcs Williams and Hawkings' [38] stress tensor is introduced after Eqn. 2.8 of their paper and is

$$\overline{T}_{ij,\,\text{Ffowcs Williams and Hawkings}} = \rho u_i u_j + p_{ij} - c_\infty^2 \left(\rho - \rho_\infty\right) \delta_{ij}. \tag{17}$$

The generalized Lighthill stress tensor of Eqn. 17 is very similar to the Lighthill stress tensor, Eqn. 16 (see [38]). For the present approach use

$$\overline{T}_{ij} = \rho u_i u_j + \tau_{ij} - \rho c^2 \delta_{ij}. \tag{18}$$

This is the first major difference between classical approaches and the present. Here, the speed of sound is local and not ambient and the density is not relative to an ambient value. The third term of the Lighthill [34] stress tensor, in any form, is a choice. Any choice can be made, but only some are useful. The choice of Lighthill [34] to introduce the term ρc_∞^2 was made to create a linear wave propagation operator for ρ, which was easily solved with a traditional Green's function. Ffowcs Williams and Hawkings [38] chose a form to find a fluctuating density. Both used c_∞, which is logical to ascertain a linear wave equation. In Eqn. 18, c is retained as the local speed of sound, not a constant ambient value, and its position within the left-hand side is important for obtaining nonlinear solutions. Also, the magnitude of ρ is used unlike Eqn. 17.

B. Formation of a Governing Equation

Now an equation is formed that is similar to an acoustic analogy, however, unlike acoustic analogies the left hand side is retained as a nonlinear operator. The approach is not an acoustic analogy because by definition acoustic analogies are linear. This is because the linearized wave operator relies on solution via of the Green's function, which is a mathematical approach for solving sets of linear partial differential equations. Note the first and second terms of Eqn. 18 appear in the second term of Eqn. 15. The third term is chosen so that a wave equation will be formed involving ρ and c. In the second term of Eqn. 15, insert the generalized form of Eqn. 18 for $\rho u_i u_j$ and τ_{ij} and add $c^2 \rho \delta_{ij}$ to balance the equation. Then subtract $\partial/\partial x_i$ of Eqn. 15 with the insertion described previously from $\partial/\partial t$ of Eqn. 14.

The equation is rearranged to find

$$\underbrace{\frac{\partial^2\overline{\rho}}{\partial t^2} - \frac{\partial\overline{\rho c^2}\delta_{ij}}{\partial x_i \partial x_j}}_{\text{propagator}} = \underbrace{\frac{\partial\overline{T}_{ij}}{\partial x_i \partial x_j}}_{\mathcal{S}_T} - \underbrace{\frac{\partial}{\partial x_i}\left(\tau_{ij}\delta(f)\frac{\partial f}{\partial x_j}\right)}_{\mathcal{S}_l} + \underbrace{\frac{\partial}{\partial t}\left(\rho v_i \delta(f)\frac{\partial f}{\partial x_i}\right)}_{\mathcal{S}_t}. \tag{19}$$

For ease of analysis, define the right hand side term by term as $\mathcal{S}_T = \frac{\partial\overline{T}_{ij}}{\partial x_i \partial x_j}$, $\mathcal{S}_l = -\frac{\partial}{\partial x_i}\left(\tau_{ij}\delta(f)\frac{\partial f}{\partial x_j}\right)$, and $\mathcal{S}_T = \frac{\partial}{\partial t}\left(\rho v_i \delta(f)\frac{\partial f}{\partial x_i}\right)$. Here, $\mathcal{W} = \mathcal{S}_T + \mathcal{S}_l + \mathcal{S}_t$ as the right hand side. The subscripts stand for Lighthill stress, loading, and thickness terms, respectively, and correspond to the traditional linear description in the aeroacoustics community. However, for problems at hand, it is not possible or appropriate to find a nonlinear solution from any single term. Solutions cannot be found through superposition. For now on, refer to the left hand side of Eqn. 19 as the propagator. From this point forward and for convenience, the notation of generalized functions is removed.

Note in Eqn. 19, Lighthill [34] originally assumed that c on the left hand side was the ambient value c_∞. Ffowcs Williams and Hawkings [38] did this also in Eqn. 2.8 of their paper, by moving c. Thus, both Lighthill [34] and Ffowcs Williams and Hawkings [38] had the same left hand side, except the latter was generalized. This allowed them to use the theory of Green's functions [43] with linear partial differential equations to solve the acoustic analogy. The necessary change here is to leave c within the partial derivative of the left hand side of Eqn. 19. For the present approach, it is a fortunate coincidence that c^2 is present, as c is a measure of compressibility of a fluid (see Shapiro [44]).

Remember, to solve Lighthill's original acoustic analogy, one would need to know the complete solution of the Navier-Stokes equations in all space and time. That is, part of the unknown solution of Lighthill's approach requires knowing density on both the left and right hand side (see density in T_{ij} of Lighthill [34]). Lighthill assumed the right hand side is known and treated it as a source. Here, treat the right hand side as a boundary value problem, and retain the same set of unknowns, but elect to leave one extra on the left hand side, which is c.

C. Proposed Specific Solution

One class of specific closed-form solutions for ρ is proposed as a function of space and time. Here, a new approach is used relative to previous investigators such as Lighthill [34], Oseen [32], or Ffowcs Williams and Hawkings [38]. Let the static density in the flow-field be

$$\rho(\boldsymbol{x}, t) = \int_{-\infty}^{\infty}\int_{0}^{\mathcal{P}} \mathcal{M}\mathcal{W} d\tau d\boldsymbol{y}, \tag{20}$$

where $\mathcal{M}$ is an unknown generalized function, $\mathcal{P}$ is the modified time to integrate (t or a factor of t depending on the

problem), $\boldsymbol{x}$ represents the observer vector, $\boldsymbol{y}$ represents the source vector, and τ is source time. The difficulty is now to ascertain these unknown generalized functions and limit of integration that also satisfies Eqn. 19, the energy equation, and gas law.

Equation 20 involves integration over space and time for the density. The equation is written in a direct way to satisfy Eqn. 19. That is specifically, if $\rho(\boldsymbol{x}, t)$ is placed in Eqn. 19, with appropriately chosen integrand then the residual error will be zero. It is an assumption that the solution exists in this form, and contains the essential mathematical elements of Oseen [32] Eqn. 5, Browder and Kato, and Lighthill [34] Eqn. 6, and Whitham [8] Eqn. 1. In particular, in Oseen [32] the closed-form solution involves both initial and boundary conditions that depend on integrands that are evaluated as the flow-field evolves. The generalized function $\mathcal{M}$ might be compared to Oseen's tensor as in Eqn. 5. It is multiplying a known source function or particular nonlinear flow-field state, which is represented as $\mathcal{W}$ in the present formulation. However, the present formulation has a much more complicated form than the terms involving $u_i \partial_i \boldsymbol{u}$ of Oseen [32]. Eqn. 20 is similar to [34], Lighthill's original acoustic analogy that relies on a Green's function for the solution. Unlike Lighthill [34], the present approach uses $\mathcal{M}$ in place of a Green's function, but as the present approach is nonlinear the function $\mathcal{M}$ and $\mathcal{W}$ are not truly separable like a Green's function and a nonlinear right hand source. Combined they represent an integrand that will result in an analytical solution for density. Only a portion of the product is known via boundary and initial conditions in the form of $\mathcal{W}$. Though knowledge of $\mathcal{W}$ is present from the formulation of the problem from Eqn. 19, it is not really possible to separate $\mathcal{W}$ from $\mathcal{M}$ for a particular problem like in linear theory. If separation or a breakdown of $\mathcal{M}$ is possible, then the breakdown presently eludes the author. Finally, Eqn. 20 must also recover the predictions of Whitham [8], as the motivation for the present theory is to create a nonlinear near-field sonic boom prediction theory.

The difficulty for finding a solution is ascertaining $\mathcal{M}$, $\mathcal{P}$, and $\mathcal{W}$. Then, placing the resultant solution for all field-variables back into the original Eqns. 7, 8, 10, 13, and 20. For all these equations, the residual must be exactly zero, or the specific analytical solution is not correct.

Here, restrict the spatial location of predictions to the near-, mid-, and far-field. Through knowledge of the density field $\rho(\boldsymbol{x}, t)$, it is possible to construct the other unknown field-variables using traditional flow theory. Closed-form solutions for $\boldsymbol{u}$, p, and T can be constructed. Construction of the generalized function $\mathcal{M}$ is very complicated. A general discussion of its construction is shown in the next subsection and specific examples with justification are shown in the prediction section.

Figure 2 shows a simplified or applied version of Fig. 1. Region 1 represents the flow-field. Region 2 is within the aerodynamic body. The function f will be less than or equal to zero within the body and greater than zero outside. The aerodynamic body will be defined by creation of a tailored f. The prediction vector $\boldsymbol{x}$ and source vector $\boldsymbol{y}$ are shown in the figure. In this analysis, the aerodynamic body will move at a velocity $\boldsymbol{v}$. Though the body can accelerate and maneuver, these cases are not presently considered. The ambient or atmospheric conditions for an external aerodynamics

problem are denoted with subscript ∞. For all analysis, the origin of the domain at time $\tau = 0$ will correspond to the leading edge or tip of the body being examined. In this analysis, the vectors $\boldsymbol{x}$ and $\boldsymbol{y}$ are fixed to the origin. That is, the coordinates are not attached to the body. As time progresses, the aerodynamic body translates across the domain. Furthermore, the source time is denoted by τ, and the observer time is denoted by t.

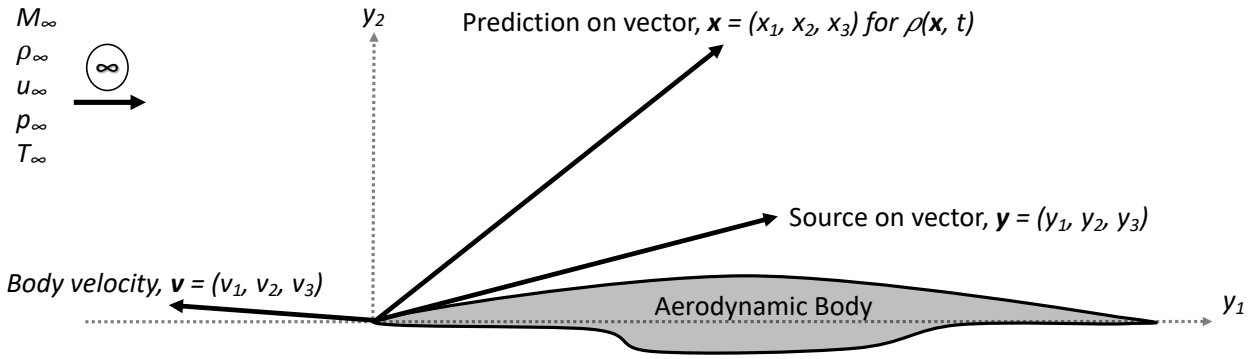

Fig. 2 Problem formulation applied to high-speed aerodynamic bodies.

Equation 20 has a very similar form relative to the closed-form solutions via a Green's function. The approach traditionally involves a convolution integral between a Green's function and the source term. In Lighthill's approach, this involves the Green's function, g, of the three-dimensional wave equation and the double divergence of the Lighthill stress tensor, T_{ij}. Typically, the free-space Green's function for Lighthill's approach involves a δ function divided by $4\pi r$, where r is the propagation distance from source to observer. Here, the double divergence of T_{ij} represents the source term of acoustic radiation. Integration for the acoustic mass density results from space and time integration. Analysis of Green's functions and their properties are not applicable to the presently proposed approach.

The unknown function $\mathcal{M}$ is not a Green's function, g, because the present approach solves a nonlinear problem as observed on the left hand side of Eqn. 19. The function $\mathcal{M}$ does not have properties like a Green's function. Also, as will be shown in the results section, $\mathcal{W}$ cannot be evaluated in separate parts as in traditional aeroacoustic analysis, because of interest in predicting nonlinear wave propagation and not linear wave propagation. Furthermore, one cannot separate $\mathcal{M}$ from $\mathcal{W}$ in a linear fashion. In the predictions shown below, the Lighthill stress tensor, T_{ij}, is removed from the source term to recover traditional compressible flow theory solutions.

One might wonder if there is a proof that the integral is convergent, if it exists, and if it is unique. It will be shown for certain cases that the solution exists by presenting predictions, which correspond to classical theory. No claims of uniqueness for certain cases exist, however, certain cases like oblique shock waves are not unique solutions. For example, the strong and weak shock wave solution will be recovered, which shows the solution is not unique. Thus, solutions are likely not unique and others likely exist. It is not claimed that this paper proposes a general solution, but only specific solutions for the benefit of practical predictions of hyperbolic flow-fields.

D. Construction of Complicated Solutions

For simple flows-fields, shown in the next section, Eqn. 20 can often be integrated directly. More complicated solutions for density can be derived by multiplying ratios of density, which can also be found by Eqn. 20. To construct complicated fields of density the following equation is proposed

$$\rho(\boldsymbol{x}, t) = \rho_\infty \prod_{i=1}^{\infty} \frac{\rho_{i+1}}{\rho_i} \in \mathcal{M}_i, \tag{21}$$

where ρ_∞ represents the quiescent flow-field. Intersections of solutions are those where radiated waves interact. Intersections, illustrated in the prediction section for two cases, demonstrate that Eqn. 21 must be used with care. Also, by creating simple specific solutions, very complicated solutions can be found without having to directly integrate Eqn. 20 for a complicated geometry. Equation 20 must only be applied in regions without interacting $\mathcal{M}$.

E. Practical Construction of Solutions

A practical approach is proposed to construct analytical solutions. Refer to Fig. 3. The problem definition involves specifying boundary conditions that include ambient Mach number, density, velocity, pressure, and temperature. For sonic boom problems, altitude and propagation distance will be included. Furthermore, the specification of the prediction vector $\boldsymbol{x}$ must be defined, which is fixed relative to the coordinate frame. The aerodynamic body is expected to move through the field at velocity $\boldsymbol{v}$ relative to the coordinate frame and origin. At source time $\tau = 0$, the leading edge of the aerodynamic body is at the origin.

Next, the boundary condition or boundary value problem must be specified. One of the boundaries is the ambient flow-field itself, as previously described, and the second is the geometry of the aerodynamic body. The function f describes the surface, where $f > 0$ describes the flow-field and $f < 0$ describes the interior of the aerodynamic body. It is generally composed of products of the Heaviside function. A typical calculation includes the static pressure estimate on the body surface. Also, it is optional to include an estimation of the boundary layer, be it laminar or turbulent, as part of the problem, which can be included in the Navier-Stokes tensor source term. To recover classical solutions in compressible flow, this is not required and will not be presented in the present work. On the aerodynamic body, the surface velocity is required, which is $\boldsymbol{v}$, an estimation of the static pressure p, the surface density ρ, and any knowledge of viscous terms if viscous effects are to be included.

Function f is constructed from generalized functions. Generally, the Heaviside function is used to construct the aerodynamic body shape. Examples of its construction are shown in this paper. In particular, f is a function of $\boldsymbol{y}$ and τ, because its position is moving relative to the origin of the coordinate system. Complicated smooth or sharp surfaces can be modeled this way. f will be greater than zero outside the surface. f must also be differentiable and integratable in $\boldsymbol{y}$.

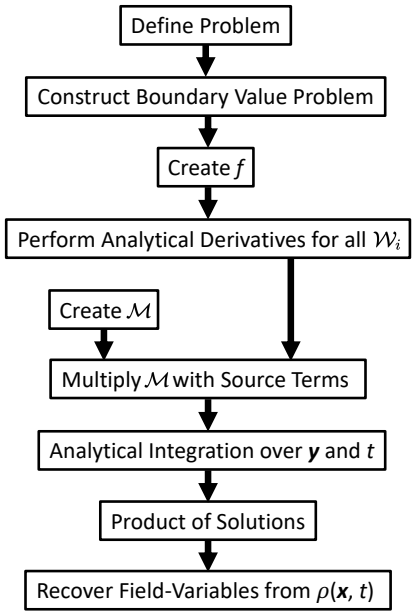

Fig. 3 Problem formulation applied to high-speed aerodynamic bodies.

The resultant multiplication of f after its derivatives are performed with source terms can sometimes be integrable, though there is no guarantee. For complicated geometries, it is fortuitous that terms are integratable.

Now that f is defined, its spatial derivatives are performed in each direction y_i for $i = 1$ to 3. Then these derivatives are multiplied by $\delta(f)$, and further multiplied by the stress tensor, which involves only static pressure for inviscid flow, and the ambient density and aerodynamic velocity, where applicable. Subsequently, take the spatial derivatives of these resultant terms. Refer to Eqn. 19 for S_l and S_t, to understand these operations. If viscosity is to be included, then form T_{ij} and perform the double divergence to find the term S_T. A most important identity for integration is $\frac{d}{dy}(H(y)) = \delta(y)$. Typically, as will be seen in specific examples forthcoming, functions involving mostly Dirac delta functions, Heaviside functions, and their derivatives or combinations thereof will be found.

For each aerodynamic problem, it is very likely that a unique $\mathcal{M}$ will exist. However, similarities between, say, compression waves and expansion waves give a strategy for finding $\mathcal{M}$. One must choose a function that yields an analytical solution. As the equations are nonlinear partial differential equations, this is not surprising. One does not know in advance if the generalized function $\mathcal{M}$ exists for a particular solution in the form of the proposed integration of $\mathcal{MW}$.

In the cases presented in the prediction section the formulation of $\mathcal{M}$ is described and certain trends appear. Because the creation of $\mathcal{M}$ is so complicated even for the simplest of cases, it is proposed that the products of solutions for density be used instead of finding tailored and specific $\mathcal{M}$, much like one would find a tailored Green's function. Product superposition is used instaed of linear superposition.

The next step in the solution construction approach is to multiply $\mathcal{M}$ with $\mathcal{W}_1$ through $\mathcal{W}_3$. Then attempt integration over time first and all three spatial source vectors $\mathcal{W}_1$ through $\mathcal{W}_3$. Through careful construction of $\mathcal{M}$, these four integrals can often be performed, and the resultant equation simplified for a closed-form analytical solution of the mass density in the field.

If the density can be predicted and if two $\mathcal{M}$ functions interact, just like two shock waves coalescing, or shock waves interacting with an expansion wave, or two expansion waves interacting, or any other type of radiating wave interaction, then the product of ratio of density change is used. This is the meaning of Eqn. 21, which represents products of simplified solutions. For example, shock or expansion waves interacting yields a new and more complicated solution.

This product of simplified analytical solutions produces new, more complicated analytical solutions. This will be illustrated in the prediction section. The number of products to find a continuous solution of a Prandtl-Meyer expansion wave will be infinite. However, because solutions are evaluated on a discrete computer, the number of products for an individual expansion wave must be set to a finite value. Here, this value is 1001. The value of 1001 was chosen as a balance between numerical convergence and file size generation. A numerical example is presented later to demonstrate the effect of evaluation of the number of products for a single expansion.

If an expansion wave interacts with a shock wave, for example, then the number of products of solutions will be even greater. If an expansion wave interacts with another expansion wave, then it is expected that the number of products of solutions needed to find an analytical solution to be very large and intractable for practical calculation. Therefore, this product of solution approach has been implemented in a computer program that is discussed in the next subsection to overcome these difficulties.

Once the density is known in the flow-field, it is easy to reconstruct all other field-variables. First, recognize that large portions of the near-field and far-field are isentropic, except in certain circumstances. The total properties of the flow-field can be found through isentropic regions. Density variations across isentropic regions are found through shock wave or slip relations. At locations of shock waves, the Hugoniot [45, 46] relation with perfect gas assumption is used to find the pressure change, which is

$$\frac{p_2}{p_1} = \frac{\left(\frac{\gamma+1}{\gamma-1}\right)\frac{\rho_2}{\rho_1} - 1}{\left(\frac{\gamma+1}{\gamma-1}\right) - \frac{\rho_2}{\rho_1}}. \tag{22}$$

As ρ and p are known, T can be found through the gas law via

$$\frac{T_2}{T_1} = \frac{p_2}{p_1}\frac{\rho_1}{\rho_2}, \tag{23}$$

and the gas law in other regions. Velocity is recovered from the Mach number and temperature using isentropic relations between static density and total density. The isentropic relation for ρ is

$$\frac{\rho_o}{\rho} = \left(\frac{\gamma - 1}{2} M^2 + 1\right)^{\frac{1}{\gamma - 1}}, \tag{24}$$

where ρ_o is the total density. Recall, $M = (u_i u_i)^{1/2} c^{-1} = (u_i u_i)^{1/2} (\gamma RT)^{-1/2}$. This is how the flow-field is constructed from knowledge of the mass density field.

F. Implementation into Computer Program

To construct complicated analytical solutions, a computer program named the Integral Method Program (IMP) is developed. This program predicts supersonic flow-fields defined as boundary value problems by integrating the incoming flow-field with the geometry and properties of the aerodynamic body. The program follows the same framework and the mathematics as previously depicted in Fig. 3. The program requires a geometry of the aerodynamic body consisting of local turning angles of the body on a parameterized or discretized surface. It also requires specification of the incoming supersonic flow-field. Using this input data, the program predicts the aerodynamic near-field. Additionally, the program contains a waveform parameter based sonic boom prediction subroutine (see Thomas [47]) and is also compatible with PCBOOM [48]. The program outputs the near-field and ground pressure waveform, displaying pressure as a function of time, both onscreen and in output files after post-processing. While the present paper does shows one example with a propagation solver, a primary objective of the IMP is the rapid determination of the aerodynamic near-field around slender hypersonic or supersonic bodies for sonic boom prediction.

The IMP is developed in contemporary object-oriented Fortran [49]. It runs in serial and does not depend on external libraries. An Apple M1 central processing unit running the MAC OSX operating system 14.3.1 is used to develop IMP. All calculations are performed on the same machine. For post-processing, Python 3.12 and Mathematica 13.2.1 are utilized. Paraview version 5.6 is used to examine geometries.

IMP evaluates the boundary value problem, and two boundaries are specified by the user for a calculation. The incoming flow-field represents one of the boundaries and requires specification of M_∞, p_∞, and T_∞ at a given altitude. Utilizing the ideal gas law and the definition of Mach number, the program computes u_∞ and ρ_∞. Flow inclination angles, α and β, are used to modify $\boldsymbol{u}_\infty$. The aerodynamic body's geometry constitutes the second boundary condition. The program has the ability to load either a discretized boundary consisting of points and connectivity in two-dimensions, axisymmetric coordinates, or three-dimensions. There is some limited capability to load parameterized surfaces in two-dimensional or axisymmetric coordinates.

The program reads two files when executed. The first is "input.nml," which is a Fortran namelist. This file contains

prescribed ambient boundary conditions and specifies the type of prediction. Users can specify the body's dimensionality (axisymmetric, two-dimensional, or three-dimensional), along with the aerodynamic body's length-to-thickness ratio, angles of attack and yaw, ground-level pressure and temperature, gas constant, and specific heat ratio. Additional input parameters allow for the designation of a source cylinder location around the aerodynamic body for sonic boom prediction, that requires the heading, latitude, longitude, ground reflection coefficient, and atmospheric model. Multiple atmospheric models can also be used that include uniform, US standard, and user-defined. The second file is called "input-geo.dat," and contains in ASCII format the geometry of the aerodynamic body. The first line of the file specifies the geometry type (two-dimensions, axisymmetric, or three-dimensions). Internally, all coordinates are cylindrical and are represented as x, r, and ϕ triplets. These sets represent lines along the aerodynamic body in the streamwise direction and are assumed connected in the azimuthal direction, ϕ. Axisymmetric or two-dimensional calculations only require a single set of coordinates along $\phi = 0$.

Upon executing the IMP, various output files are generated, contingent on the configuration specified within the namelist and geometry files. Typically, the program produces an aerodynamic estimation of the boundary values of the body, files containing near-field aerodynamic data, and if the sonic boom solver is enabled, files containing the ground waveform. It is also possible to obtain a ground waveform without a sonic boom solver in a quiescent atmosphere, though this has little application other than bench-marking sonic boom propagation codes.

During program execution, substantial data is displayed on the screen, including the coefficients of lift and drag. These coefficients, along with an echo of all input data to the screen, are not archived in files but are crucial for verifying that the solver operates as anticipated.

The principal output is contained in the "solution.dat" file, which is an ASCII text file in the format of the Mathematical Markup Language (MathML) [50]. This file can be examined using a text editor for simple solutions. However, complex solutions, such as those involving a diamond airfoil, generate extensive data that are challenging to interpret. This is because the solution.dat file contains mostly integrated products of many $\mathcal{M}$ and $\mathcal{W}$ functions and their interactions, which are generalized functions. There is little numerical data in the solution.dat file. Simpler solutions, like a two-dimensional oblique shock wave, are easily represented by a few lines in the output file, whereas more intricate solutions involving multiple interactions of expansion and shock waves yield large amounts of data that might span a solution domain of multiple kilometers.

The post-processing phase visualizes the predictions contained in the MathML solution.dat file. A Python script reads the solution.dat and Fortran namelist input files then creates plots directly or suitable for plotting with Mathematica. This script is particularly useful for sonic boom analysis, where it creates numerical data by applying boundary conditions specified by the user to the MathML solution.dat file. Both files include headings that describe the variables in each column, with the dimensional file detailing the axial coordinate, M, p, x, and ρ, and the normalized file contains x/c, $(\Delta p - p_\infty)/p_\infty$, and M in three columns. These files are used for generating the figures shown in the present paper. An

example ASCII post-processed file for a simple calculation is:

```
$x/c$, $\Delta p / p_\infty$, $M$
1.9804547795773524 0.0000000000000000 2.3999999999999999
1.9804547795773524 0.19857620275793714 2.2837549211426231
(Note: lines truncated due to length.)
3.0869213592825315 -0.16620619081880095 2.5162697352469978
3.1059551469233262 -0.17161298277946685 2.5204554733716447
3.3976653270186867 -0.17161298277946810 2.5204554733716460
3.3976653270186867 1.5433135341814808E-005 2.3991661136366713
```

The first line represents the variables in LaTeX format. The variables are then written in columns from the front of the vehicle to the rear in each azimuthal plane ϕ. The first column, for example, is normalized distance (axial position normalized by chord).

The IMP also provides traditional aerodynamic predictions in an output file called "output-aerobody.dat." It contains estimations of the aerodynamic properties such as coefficient of lift and drag.

The IMP is designed for efficiency, with wall clock execution times for simpler two-dimensional cases, such as those involving a shock wave and expansion, measured in seconds. More complex scenarios involving numerous interactions may require up to a few minutes on a single Apple M1 processor. Execution time of IMP is mostly limited by hard disk drive write speed.

III. Predictions

A series of predictions are presented in order of complexity, and predictions build upon one-another. The fundamental moving shock wave is recovered from a moving wall. An impulse expansion is obtained via instantaneously altering the velocity of the wall in the opposite direction. The fundamental moving surface solutions are then used to find the closed-form solutions for the oblique shock wave and Prandtl-Meyer expansion wave. By combining these fundamental solutions, Eqn. 21 is used to construct more complicated solutions. An example solutions where no interactions of $\mathcal{M}$ occur is presented for a wedge-wall-flare body. A solution for a double wedge is then constructed, which includes a single interaction from two oblique shock waves. Finally, an infinite interaction solution is presented for the classic diamond airfoil flow-field.

The same ambient conditions are used throughout the paper unless otherwise stated. Ambient conditions are $p_\infty = 101,325$ Pa, $T_\infty = 293$ K, $\gamma = 7/5$, $R = 287$ J/(kg K), and $\rho_\infty = p_\infty R^{-1} T_\infty^{-1} \approx 1.20494$ kg/m^3.

A. Normal Shock Wave

The first case examined is of fundamental nature, where a moving wall is impulsively started with a velocity v_2 and creates a moving shock wave. The geometry is illustrated in Fig. 4. The coordinate system is denoted by y_1 and y_2. The wall moves at a velocity v_2 in the y_2 direction. The observer position is represented by the vector $\boldsymbol{x}$, and the source position is represented by the vector $\boldsymbol{y}$. Here, y_1 is only shown for convenience, and the problem is only dependent on the spatial coordinate x_2 and time t. As the wall moves from its initial position $y_2 = 0$ at a finite velocity v_2, a moving normal shock wave, labeled "wave," propagates in the y_2 direction. The goal is to find the analytical solution for $\rho(y_2, t)$. The words source and observer are used due to tradition, but as this is a nonlinear problem everything is "lumped" into one term.

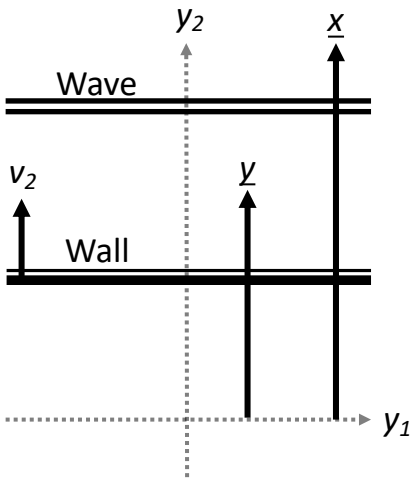

Fig. 4 Diagram of a moving wall with radiated wave.

Now construct the boundary value problem for aerodynamic properties on the boundary. On the boundary $f = 0$. Construct f as

$$f = \mathcal{H}\left[y_2 - v_2\tau\right], \tag{25}$$

where $\mathcal{H}$ is the Heaviside function, y_2 is the source position, v_2 is the velocity of the piston, and τ is the source time. This corresponds to f in Fig. 1. Note that f is constructed with a Heaviside function that represents the inviscid shock wave. Now that f is constructed, take the derivative in the y_2 direction as it is a single spatial dimensional problem, which corresponds to the partial derivative operation on the right hand side of Eqn. 19. This operation yields

$$\frac{\partial f}{\partial y_2} = \delta\left[y_2 - v_2\tau\right], \tag{26}$$

where δ is the Dirac delta function. The source functions of Eqn. 19 on the right hand side are now constructed. The function f is inserted into $\mathcal{S}$. For the present case $\mathcal{W}$ is

$$\begin{aligned}\mathcal{W}_2 = -\frac{\partial}{\partial y_i}\left(\tau_{ij}\delta(f)\frac{\partial f}{\partial y_j}\right) =& p\delta\left[\mathcal{H}[y_2 - v_2\tau]\right]\delta'[y_2 - v_2\tau] \\ &+ p\delta[y_2 - v_2\tau]^2\delta'\left[\mathcal{H}[y_2 - v_2\tau]\right]\end{aligned} \tag{27}$$

and

$$\begin{aligned}\mathcal{W}_3 = \frac{\partial}{\partial\tau}\left[\rho v_2\delta(f)\frac{\partial f}{\partial y_2}\right] =& -\rho v_2^2\delta\left[\mathcal{H}\left[y_2 - v_2\tau\right]\right]\delta'\left[y_2 - v_2\tau\right] \\ &- \rho v_2^2\delta\left[y_2 - v_2\tau\right]^2\delta'\left[\mathcal{H}\left[y_2 - v_2\tau\right]\right].\end{aligned} \tag{28}$$

Prime denotes the partial derivative with respect to τ. Here, variables such as ρ and p are known on the right hand side, as they are part of the boundary condition. These terms represent the right hand side of Eqn. 19. For this specific problem, ρ and p do not change on the boundary. Note there is no $\mathcal{W}_1$ term because there is no turbulence on the face of the piston. Also, to recover a specific analytical solution, the $\mathcal{W}_1$ function is not needed. Before integration, the term $\mathcal{M}$ must be found. The term $\mathcal{M}$ for this problem is as function for the region of influence. It is a combined source-propagation function when multiplied by $\mathcal{W}$. In nonlinear solutions, the source and propagation functions are likely to be inseparable. The function must be valid in the region of influence from the piston and the core dynamics of the velocity and density rise due to the movement of the boundary condition. The $\mathcal{M}$ function is deduced as

$$\mathcal{M} = \frac{2v_2\left(\rho_\infty + (\rho - \rho_\infty)\mathcal{H}\left[tv_2\frac{\rho}{\rho_\infty}\left(\frac{\rho}{\rho_\infty} - 1\right)^{-1} - x_2\right]\right)}{p - \rho v_2^2}. \tag{29}$$

Note that the variable x_2 is the observer location relative to the origin. Within the Heaviside function, the first term reduces to a distance that the wave has traveled and is a function of the time, velocity, and density rise across the wave. It is consistent with moving shock wave theory (see Shapiro [44] for details). Using Eqn. 20 and substitution of $\mathcal{M}$ and $\mathcal{W}$, find

$$\rho\left(\boldsymbol{x},t\right)=\int_{-\infty}^{\infty}\int_{0}^{t}\left(\frac{2v_2\left(\rho_\infty+(\rho-\rho_\infty)\mathcal{H}\left[tv_2\frac{\rho}{\rho_\infty}\left(\frac{\rho}{\rho_\infty}-1\right)^{-1}-x_2\right]\right)}{p-v_2^2\rho}\right)$$
$$\times\Big(p\delta[\mathcal{H}[y_2-v_2\tau]]\delta'[y_2-v_2\tau]+p\delta[y_2-v_2\tau]^2\delta'[\mathcal{H}[y_2-v_2\tau]] \tag{30}$$
$$-\rho v_2^2\delta\left[\mathcal{H}\left[y_2-v_2\tau\right]\right]\delta'\left[y_2-v_2\tau\right]$$
$$-\rho v_2^2\delta\left[y_2-v_2\tau\right]^2\delta'\left[\mathcal{H}\left[y_2-v_2\tau\right]\right]\Big)d\tau d\boldsymbol{y}.$$

Now, directly seek a solution through analytical integration. First, integrate with respect to τ via separating the integration into two integrals involving terms $\mathcal{W}_2$ and $\mathcal{W}_3$. The $\mathcal{W}_2$ integration with τ is

$$\begin{aligned}\mathcal{I}_{2\tau}&=\int_0^t\mathcal{M}\left(p\delta[\mathcal{H}[y_2-v_2\tau]]\delta'[y_2-v_2\tau]+p\delta[y_2-v_2\tau]^2\delta'[\mathcal{H}[y_2-v_2\tau]]\right)d\tau\\&=-\mathcal{M}\Bigg(\Bigg(2\Big(p\delta[y_2]\delta[\mathcal{H}[y_2]]-p\delta\Big[y_2-t\frac{\rho}{\rho_\infty}\left(\frac{\rho}{\rho_\infty}-1\right)^{-1}v_2\Big]\\&\quad\times\delta\Big[\mathcal{H}\Big[y_2-t\frac{\rho}{\rho_\infty}\left(\frac{\rho}{\rho_\infty}-1\right)^{-1}v_2\Big]\Big]\Big)\\&\quad\times\Big((\rho-\rho_\infty)\mathcal{H}\Big[t\frac{\rho}{\rho_\infty}\left(\frac{\rho}{\rho_\infty}-1\right)^{-1}v_2-x_2\Big]+\rho_\infty\Big)\Big)(p+\rho v_2^2)^{-1}\Bigg).\end{aligned} \tag{31}$$

The $\mathcal{W}_3$ integration with τ is

$$\begin{aligned}\mathcal{I}_{3\tau}&=\int_0^t\mathcal{M}\Big(-\rho v_2^2\delta\left[\mathcal{H}\left[y_2-v_2\tau\right]\right]\delta'\left[y_2-v_2\tau\right]\\&\quad-\rho v_2^2\delta\left[y_2-v_2\tau\right]^2\delta'\left[\mathcal{H}\left[y_2-v_2\tau\right]\right]\Big)d\tau\\&=-\mathcal{M}\Bigg(\frac{1}{p+\rho v_2^2}\Big(2v_2\Big((\rho-\rho_\infty)\mathcal{H}\Big[t\frac{\rho}{\rho_\infty}\left(\frac{\rho}{\rho_\infty}-1\right)^{-1}v_2-x_2\Big]+\rho_\infty\Big)\\&\quad\times\Big(\rho v_2\delta\Big[y_2-t\frac{\rho}{\rho_\infty}\left(\frac{\rho}{\rho_\infty}-1\right)^{-1}v_2\Big]\delta\Big[\mathcal{H}\Big[y_2-t\frac{\rho}{\rho_\infty}\left(\frac{\rho}{\rho_\infty}-1\right)^{-1}v_2\Big]\Big]\\&\quad-\rho v_2\delta[y_2]\delta[\mathcal{H}[y_2]]\Big)\Big)\Bigg).\end{aligned} \tag{32}$$

Here, the result of these integrals $\mathcal{I}_{2\tau}$ and $\mathcal{I}_{3\tau}$ are designated to indicate integration with respect to τ for terms two and three, respectively. The next step is to integrate $\mathcal{I}_{2\tau}$ and $\mathcal{I}_{3\tau}$ over y_2 from negative infinity to infinity.

The first integral results in

$$\begin{aligned}\mathcal{I}_{2y} &= \int_{-\infty}^{\infty} \mathcal{I}_{2\tau} dy_2 \\ &= \frac{-\mathcal{M}\left(2p\mathcal{H}[0]\left(\rho_\infty + (\rho-\rho_\infty)\mathcal{H}\left[t\frac{\rho}{\rho_\infty}\left(\frac{\rho}{\rho_\infty}-1\right)^{-1} v_2 - x_2\right]\right)\right)}{p+\rho v_2^2} \\ &+ \frac{2p\left(\rho_\infty + (\rho-\rho_\infty)\mathcal{H}\left[t\frac{\rho}{\rho_\infty}\left(\frac{\rho}{\rho_\infty}-1\right)^{-1} v_2 - x_2\right]\right)}{p+\rho v_2^2}\end{aligned} \tag{33}$$

and the second results in

$$\begin{aligned}\mathcal{I}_{3y} &= \int_{-\infty}^{\infty} \mathcal{I}_{3\tau} dy_2 \\ &= \frac{-\mathcal{M}\left(2\rho v_2^2\mathcal{H}[0]\left(\rho_\infty + (\rho-\rho_\infty)\mathcal{H}\left[t\frac{\rho}{\rho_\infty}\left(\frac{\rho}{\rho_\infty}-1\right)^{-1} v_2 - x_2\right]\right)\right)}{p+\rho v_2^2} \\ &+ \frac{2\rho v_2^2\left(\rho_\infty + (\rho-\rho_\infty)\mathcal{H}\left[t\frac{\rho}{\rho_\infty}\left(\frac{\rho}{\rho_\infty}-1\right)^{-1} v_2 - x_2\right]\right)}{p+\rho v_2^2}.\end{aligned} \tag{34}$$

Note the following properties used for integration

$$\delta\left[\mathcal{H}[x]\right] = \mathcal{H}[-x] \tag{35}$$

and

$$\int \delta[x] f(x) dx = f(0)\mathcal{H}[x]. \tag{36}$$

For the Heaviside function, adapt $\mathcal{H}[0] = 1/2$. Adding the integrations of $\mathcal{I}_{2y}$ and $\mathcal{I}_{3y}$ yields ρ. After simplification the density is a function of x and t

$$\rho\left(\boldsymbol{x}, t\right) = (\rho-\rho_\infty)\mathcal{H}\left[t v_2 \frac{\rho}{\rho_\infty}\left(\frac{\rho}{\rho_\infty}-1\right)^{-1} - x_2\right] + \rho_\infty, \tag{37}$$

which is the closed-form analytical solution for the density field. Here, $t \geq 0$. From the density relation for the present problem, the ratio of pressures is found from the Hugoniot relation, Eqn. 22. The ideal gas law, Eqn. 13, is then used to find T. The velocity through the entire flow-field is already known from the surface to the shock wave surface, which is v_2 between the surface and the wave, due to continuity.

Equation 37 is the solution of a boundary value problem. Knowledge of the solution at the boundary for the present case is ascertained by first choosing v_2. Everything on the right hand side is known. In Fig. 5, five normal shock waves moving at Mach numbers, $M_s = 3/2$, 2, 3, 4, and 5 are predicted. Here, the M_s indicates the Mach number of the moving shock wave. Piston velocities are $v_2 \approx 514.671$ m/s, 686.229 m/s, 1029.34 m/s, 1372.46 m/s, and 1715.57 m/s, respectively. Predictions are performed at $t \approx 0.001947$ s, $t \approx 0.00211038$ s, $t \approx 0.00226565$ s, $t \approx 0.00233158$ s, and $t \approx 0.00236478$ s, respectively.

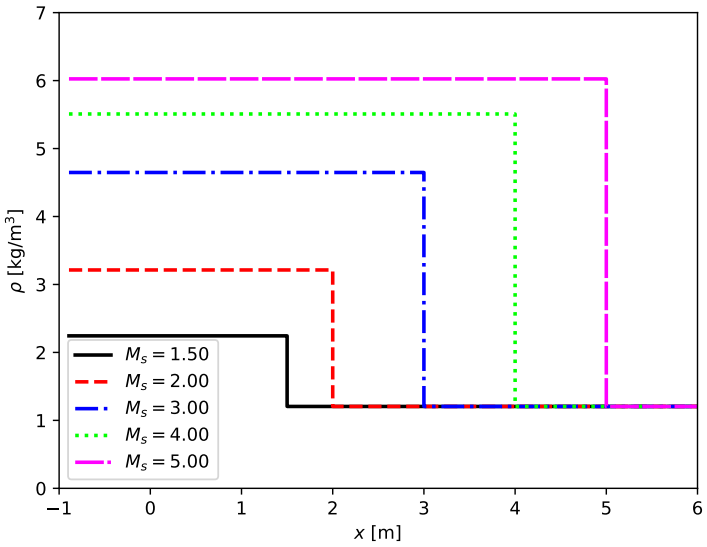

Fig. 5 Density of moving shock waves from moving wall at times t.

B. Impulse Expansion Wave

The expansion wave is now examined, which is the opposite problem of the compression wave. The piston or wall in Fig. 4 moves in the opposite direction of the radiated wave. The analyses is almost identical to the compression problem. First, examine a very small change in velocity of the wall. The function f remains the same and is

$$f = \mathcal{H}[y_2 - v_2\tau], \tag{38}$$

and restrict $v_2 < 0$ and $t \geq 0$, which indicates that the surface is moving in the negative y_2 direction. A new $\mathcal{M}$ is proposed for the expansion wave as

$$\mathcal{M} = \mathcal{H}\left[x_2 - M_\infty c_\infty t \tan 2^{-1}\left[\sin^{-1}\left(\frac{1}{M_\infty}\right)\right]\right], \tag{39}$$

where $\tan 2^{-1}$ yields the angle in the correct quadrant without causing a singularity in a computer implementation of the equation. Integrations are almost the same as the compression example. Now, find the density field due to a very weak expansion as

$$\rho\left(\boldsymbol{x}, t\right) = (\rho - \rho_\infty)\mathcal{H}\left[M_\infty c_\infty t \tan 2^{-1}\left[\sin^{-1}\left(\frac{1}{M_\infty}\right)\right] - x_2\right] + \rho_\infty. \tag{40}$$

Equation 40 is evaluated numerically to illustrate the solution. Let the wall of Fig. 4 initially move relative to the undisturbed medium at initial Mach numbers $M = 1, 3/2, 2$, and 3. The wall instantaneously changes its M by 1% in the negative y_2 direction. The change is isentropic as it is an expansion. Assume the change generates a single expansion wave as the change in velocity is very small. Figure 6 shows the resultant flow-fields at times $t \approx 0.00185542$ s, $t \approx 0.00325849$ s, $t \approx 0.00504803$ s, and $t \approx 0.0082434$ s, respectively. These times are chosen so that waves are aligned with corresponding x positions with respect to M_s. The x-axis is x in m, and the y-axis is ρ in kg/m^3, predicted by Eqn. 40.

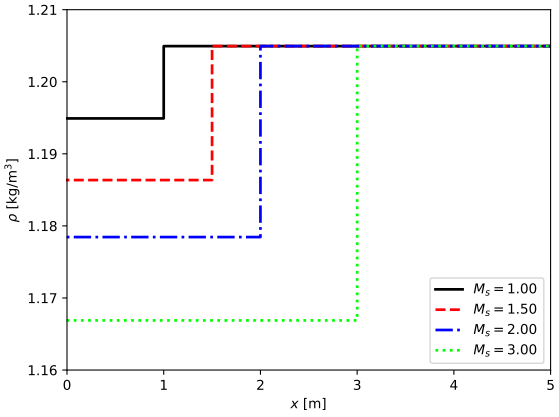

Fig. 6 Density of impulse expansion wave from moving wall at times t.

C. Planar Oblique Shock Wave

With knowledge of the wall compression case, it is possible to solve the oblique shock wave problem. Figure 7 illustrates the problem. The body moves at negative M_∞ relative to the y_1 direction. The flow is turned by an angle θ deg. A resultant shock wave is attached to the body, where the flow is instantaneously turned. A shock wave radiates at angle β relative to the incoming flow direction. As previously noted, the source vector is $\boldsymbol{y}$, and the prediction vector for ρ is $\boldsymbol{x}$. The traditional decomposition of the velocity vector pre- and post-shock wave are shown at 1 and 2 in Fig. 7. For details of the traditional derivation of the problem see Meyer [51] or Shapiro [44].

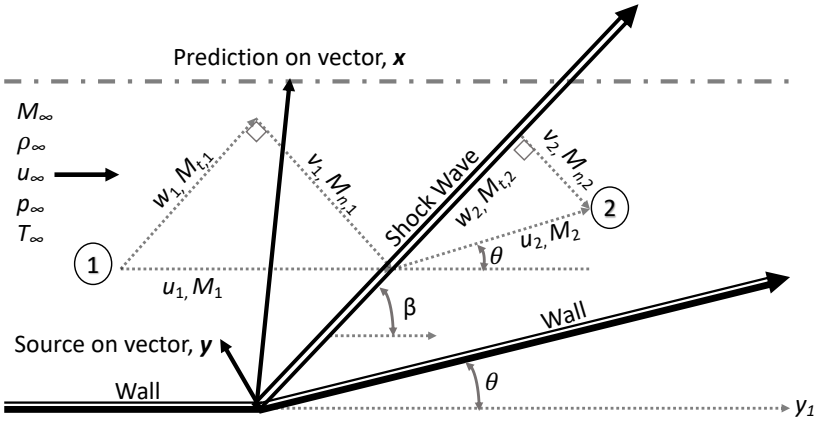

Fig. 7 Diagram of an oblique shock wave.

By examining Fig. 7, it is clear that the region above the wall is the field. The region below the wall is the interior of the aerodynamic body, corresponding to Regions 1 and 2, respectively. Construction of f is written via multiplication of two Heaviside functions. One for the wall at angle θ and another for the wall parallel to y_1. The f function for the wedge is

$$f = \mathcal{H}[y_2 - y_1 \tan\theta - M_\infty c_\infty \tau \tan\theta]\mathcal{H}[y_2]. \tag{41}$$

Construct the derivatives with respect to f yields

$$\frac{\partial f}{\partial y_1} = -\delta\left[y_2 - y_1 \tan\theta - c_\infty M_\infty \tau \tan\theta\right]\mathcal{H}[y_2]\tan\theta \tag{42}$$

and

$$\begin{aligned}\frac{\partial f}{\partial y_2} =&\delta[y_2 - y_1\tan\theta - c_\infty M_\infty \tau\tan\theta]\mathcal{H}[y_2]\\ &+\delta[y_2]\mathcal{H}[y_2 - y_1\tan\theta - c_\infty M_\infty\tau\tan\theta].\end{aligned} \tag{43}$$

Constructing the sources $\mathcal{W}$ yields

$$\begin{aligned}\mathcal{W}_{21} =& -\frac{\partial}{\partial y_1}\left(\tau_{11}\delta(f)\frac{\partial f}{\partial y_1}\right)\\ =&p\tan^2\theta\delta[y_2 - y_1\tan\theta - c_\infty M_\infty\tau\tan\theta]^2\\ &\times\delta'\left[\mathcal{H}[y_2 - y_1\tan\theta - c_\infty M_\infty\tau\tan\theta]\right]\\ &+p\tan^2\theta\delta\left[\mathcal{H}[y_2 - y_1\tan\theta - c_\infty M_\infty\tau\tan\theta]\right]\\ &\times\delta'[y_2 - c_\infty M_\infty\tau\tan\theta - y_1\tan\theta],\end{aligned} \tag{44}$$

$$\begin{aligned}\mathcal{W}_{22} =& -\frac{\partial}{\partial y_2}\left(\tau_{22}\delta(f)\frac{\partial f}{\partial y_2}\right)\\ =&p\delta[y_2 - y_1\tan\theta - c_\infty M_\infty\tau\tan\theta]^2\\ &\times\delta'\left[\mathcal{H}[y_2 - y_1\tan\theta - c_\infty M_\infty\tau\tan\theta]\right]\\ &+p\delta\left[\mathcal{H}[y_2 - y_1\tan\theta - c_\infty M_\infty\tau\tan\theta]\right]\\ &\times\delta'[y_2 - c_\infty M_\infty\tau\tan\theta - y_1\tan(\theta)],\end{aligned} \tag{45}$$

$$\begin{aligned}\mathcal{W}_{31} =&\frac{\partial}{\partial\tau}\left[\rho v_1\delta(f)\frac{\partial f}{\partial y_1}\right]\\ =&c_\infty M_\infty\rho v_1\tan^2\theta\delta[y_2 - y_1\tan\theta - c_\infty M_\infty\tau\tan\theta]^2\\ &\times\delta'\left[\mathcal{H}[y_2 - y_1\tan\theta - c_\infty M_\infty\tau\tan\theta]\right]\\ &+c_\infty M_\infty\rho v_1\tan^2\theta\delta\left[\mathcal{H}[y_2 - y_1\tan\theta - c_\infty M_\infty\tau\tan\theta]\right]\\ &\times\delta'[y_2 - c_\infty M_\infty\tau\tan\theta - y_1\tan\theta],\end{aligned} \tag{46}$$

and

$$
\begin{aligned}
\mathcal{W}_{32} =& \frac{\partial}{\partial \tau}\left[\rho v_2 \delta(f)\frac{\partial f}{\partial y_2}\right] \\
=& -c_\infty M_\infty \rho v_2 \tan\theta \delta[y_2 - y_1\tan\theta - c_\infty M_\infty \tau\tan\theta]^2 \\
& \times \delta'\left[\mathcal{H}[y_2 - y_1\tan\theta - c_\infty M_\infty \tau\tan\theta]\right] \\
& - c_\infty M_\infty \rho v_2 \tan\theta \delta\left[\mathcal{H}[y_2 - y_1\tan\theta - c_\infty M_\infty \tau\tan\theta]\right] \\
& \times \delta'[y_2 - c_\infty M_\infty \tau\tan\theta - y_1\tan\theta].
\end{aligned} \tag{47}
$$

For the sources, write subscripts 21, 22, 31, and 32, which indicate the second term in the y_1 direction, second term in the y_2 direction, third term in the y_1 direction, and third term in the y_2 direction, respectively. The velocity of the body is based on the ambient condition

$$
v_1 = -M_\infty c_\infty \text{ m/s} \text{ and } v_2 = 0 \text{ m/s}. \tag{48}
$$

The function $\mathcal{M}$ is now formed for the oblique shock wave problem. An important clue for its formulation is based on the compression piston case. Note that in Eqn. 29, the correct analytical solution results if choosing a form that involves the densities, pressures, and Heaviside function. Equation 29 is used as a basis and modify the equation with the present definition of v_1 and v_2 as

$$
\begin{aligned}
\mathcal{M} =& \frac{-2M_\infty c_\infty}{p - (M_\infty c_\infty)^2\rho}\Big(\rho_\infty + (\rho - \rho_\infty)\mathcal{H}\Big[t\frac{2M_\infty c_\infty \cot\theta}{3(\gamma-1)M_\infty^2 + 6} \\
& \times \left(M_\infty^2 + T_1\cos\left(\frac{4\pi\delta}{3} + T_2\right) - 1\right) - x_2\Big]\Big),
\end{aligned} \tag{49}
$$

where term 1 (T_1) is

$$
T_1 = \left(4\left(M_\infty^2 - 1\right)^2 - 3\tan^2\theta\left(\left(\gamma^2 - 1\right)M_\infty^4 + 4\gamma M_\infty^2 + 4\right)\right)^{1/2} \tag{50}
$$

and term 2 (T_2) is

$$
T_2 = \frac{\cos^{-1}}{3}\left(\frac{\left(M_\infty^2 - 1\right)^3 - \frac{9}{8}\tan^2\theta\left((\gamma-1)M_\infty^2 + 2\right)\left((\gamma+1)M_\infty^4 + 2(\gamma-1)M_\infty^2 + 4\right)}{\left(\left(M_\infty^2 - 1\right)^2 - \frac{3}{4}\tan^2\theta\left(\left(\gamma^2-1\right)M_\infty^4 + 4\gamma M_\infty^2 + 4\right)\right)^{3/2}}\right). \tag{51}
$$

Terms T_1 and T_2 are introduced to fit the equation on the page. Multiplying $\mathcal{M}$ with the source terms $\mathcal{W}$ results in many terms. Their integration over time and space uses all the same rules and process as the two previous cases. The analytical closed-form solution for ρ radiating from the wedge is

$$\begin{aligned}\rho\left(\boldsymbol{x},t\right) =&(\rho-\rho_\infty)\mathcal{H}\left[\frac{2(c_\infty M_\infty t+x_1)\cot\theta}{3(\gamma-1)M_\infty^2+6}\right.\\&\left.\times\left(M_\infty^2+\cos\left(\frac{4}{3}\pi\delta+T_2\right)T_1-1\right)-x_2\right]\mathcal{H}(x_2)+\rho_\infty.\end{aligned}\tag{52}$$

Figure 8 shows predictions of the planar oblique shock wave at $M_\infty = 3/2, 3, 5$, and 10. Deflection angles of the surface are $\theta = 5, 30, 11$, and 20 degs., respectively. Time is set for each prediction at $t = 0$ s. Flow is steady relative to the body. Like previous solutions, the body and flow-field translate at $-M_\infty c_\infty$ for positive t. Increasing or decreasing t will translate the entire solution at velocity v_1, in the negative y_1 or positive y_1 direction, respectively. Resultant wave angles β are approximately 47.890, 52.014, 20.318, and 25.818 degs., respectively. Densities after shock waves are $\rho = 1.435$, 3.816, 2.719, and 5.721 kg/m^3, respectively. These predictions correspond with traditional theory.

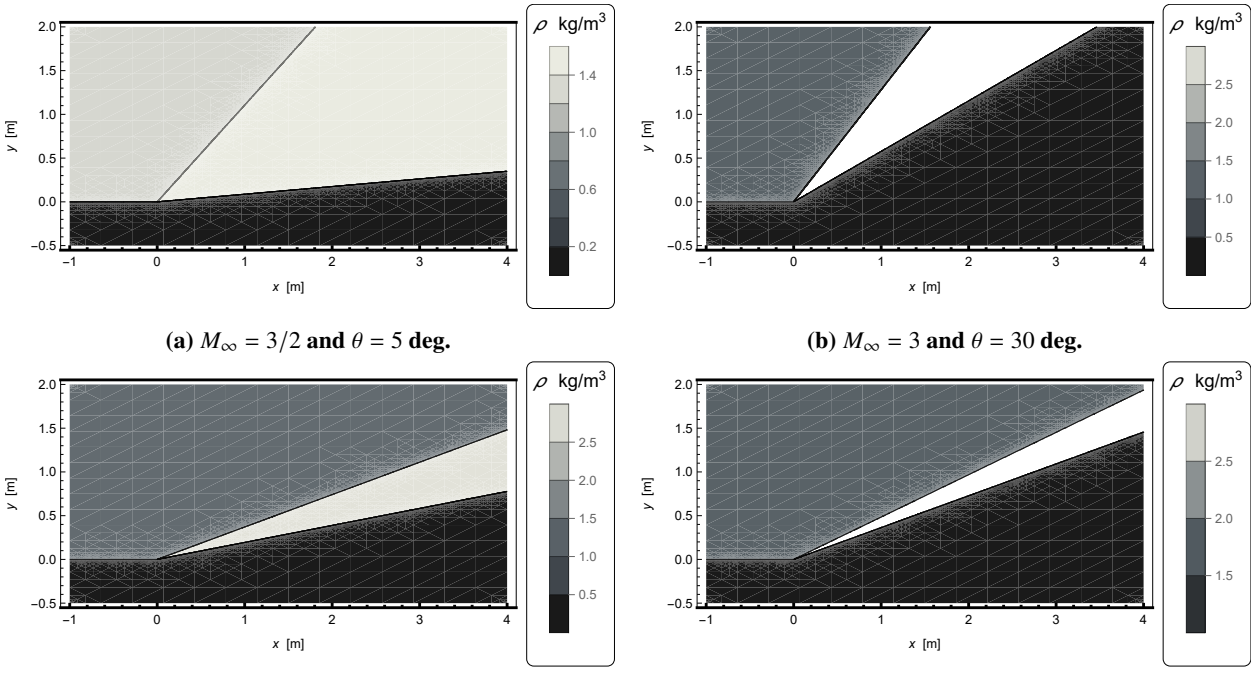

(a) $M_\infty = 3/2$ **and** $\theta = 5$ **deg.**

(b) $M_\infty = 3$ **and** $\theta = 30$ **deg.**

(c) $M_\infty = 5$ **and** $\theta = 11$ **deg.**

(d) $M_\infty = 10$ **and** $\theta = 20$ **deg.**

Fig. 8 Contours of density from attached planar oblique shock waves.

Prandtl-Meyer Expansion Wave

The next fundamental solution is for the Prandtl-Meyer [51] expansion wave. The problem is illustrated in Fig. 9. Here, an incoming flow-field at M_∞ in the y_1 direction is turned or deflected by angle θ. Note this angle is opposite of

the previously examined shock wave with turning angle $\theta \geq 0$ deg. The flow accelerates isentropically to a higher Mach number. The Prandtl-Meyer fan is bounded by Mach waves that extend from μ_1 through μ_2, which are angles relative to the incoming and out-going flow, respectively. There are an infinite number of Mach waves between the initial and final Mach waves (labeled in Fig. 9).

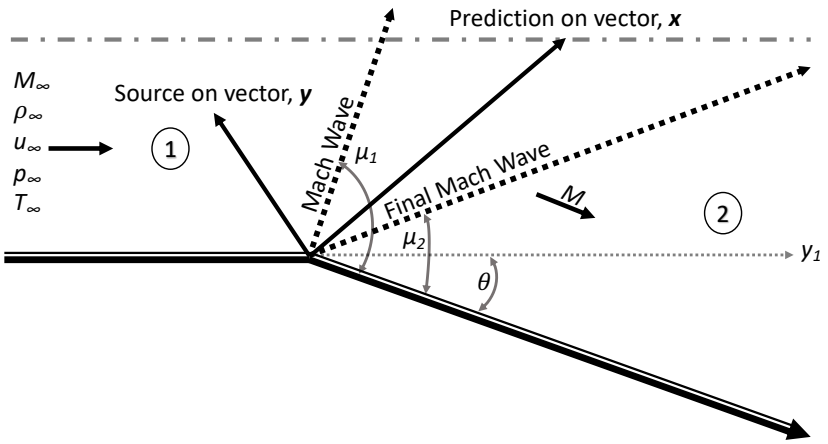

Fig. 9 Diagram of a Prandtl-Meyer expansion wave.

The f function is similar to that of the oblique shock waves, in that it can be constructed from two modified Heaviside functions that move at the velocity of the aerodynamic body. For the Prandtl-Meyer fan f is

$$f = \Big(\mathcal{H}[y_2 + (y_1 + M_\infty c_\infty \tau)\tan\theta] - 1\Big)\mathcal{H}[-y_2] + 1. \tag{53}$$

The derivatives with respect to f are

$$\frac{\partial f}{\partial y_1} = \delta\big[y_2 + (y_1 + M_\infty c_\infty \tau)\tan\theta\big]\mathcal{H}[-y_2]\tan\theta \tag{54}$$

and

$$\begin{aligned}\frac{\partial f}{\partial y_2} &= \delta\big[y_2 + (y_1 + M_\infty c_\infty \tau)\tan\theta\big]\mathcal{H}[-y_2] \\ &\quad - \big(\mathcal{H}[y_2 + (y_1 + M_\infty c_\infty \tau)\tan\theta] - 1\big)\delta[y_2].\end{aligned} \tag{55}$$

Constructing the sources $\mathcal{W}$ yields

$$
\begin{aligned}
\mathcal{W}_{21} = & -\frac{\partial}{\partial y_1}\left(\tau_{11}\delta(f)\frac{\partial f}{\partial y_1}\right) \\
& = p\mathcal{H}[-y_2]^2\tan^2\theta\delta[y_2+(y_1+M_\infty c_\infty\tau)\tan\theta]^2 \\
& \times\delta'[\mathcal{H}[-y_2](\mathcal{H}[y_2+(y_1+M_\infty c_\infty\tau)\tan\theta]-1)+1] \\
& + p\mathcal{H}[-y_2]\tan^2\theta\delta[\mathcal{H}[-y_2](\mathcal{H}[y_2+(y_1+M_\infty c_\infty\tau)\tan\theta]-1)+1] \\
& \times\delta'[M_\infty c_\infty\tan\theta\tau+y_1)+y_2],
\end{aligned}
\tag{56}
$$

$$
\begin{aligned}
\mathcal{W}_{22} = & -\frac{\partial}{\partial y_2}\left(\tau_{22}\delta(f)\frac{\partial f}{\partial y_2}\right) \\
& = p(\mathcal{H}[-y_2]\delta[y_2+(y_1+M_\infty c_\infty\tau)\tan\theta] \\
& - \delta[y_2](\mathcal{H}[y_2+(y_1+M_\infty c_\infty\tau)\tan\theta]-1))^2 \\
& \times\delta'(\mathcal{H}[-y_2](\mathcal{H}[y_2+(y_1+M_\infty c_\infty\tau)\tan\theta]-1)+1) \\
& + p\delta[\mathcal{H}[-y_2](\mathcal{H}[y_2+(y_1+M_\infty c_\infty\tau)\tan\theta]-1)+1] \\
& \times\Big(-2\delta[y_2]\delta[y_2+(y_1+M_\infty c_\infty\tau)\tan\theta] \\
& - \delta'[y_2](\mathcal{H}[y_2+(y_1+M_\infty c_\infty\tau)\tan\theta]-1) \\
& + \mathcal{H}[-y_2]\delta'[\tan\theta(M_\infty c_\infty\tau+y_1)+y_2]\Big),
\end{aligned}
\tag{57}
$$

$$
\begin{aligned}
\mathcal{W}_{31} = & \frac{\partial}{\partial\tau}\left[\rho v_1\delta(f)\frac{\partial f}{\partial y_1}\right] \\
& = \rho v_1 M_\infty c_\infty\mathcal{H}[-y_2]^2\tan^2\theta\delta[y_2+(y_1+M_\infty c_\infty\tau)\tan\theta]^2 \\
& \times\delta'[\mathcal{H}[-y_2](\mathcal{H}[y_2+(y_1+M_\infty c_\infty\tau)\tan\theta]-1)+1] \\
& + \rho v_1 M_\infty c_\infty\mathcal{H}[-y_2]\tan^2\theta\delta\big[\mathcal{H}[-y_2](\mathcal{H}[y_2+(y_1+M_\infty c_\infty\tau)\tan\theta]-1)+1\big] \\
& \times\delta'[\tan\theta(M_\infty c_\infty\tau+y_1)+y_2],
\end{aligned}
\tag{58}
$$

and

$$
\begin{aligned}
\mathcal{W}_{32} =& \frac{\partial}{\partial \tau}\left[\rho v_2 \delta(f)\frac{\partial f}{\partial y_2}\right] \\
=& \rho v_2 M_\infty c_\infty \mathcal{H}[-y_2]\tan\theta\delta[y_2 + (y_1 + M_\infty c_\infty \tau)\tan\theta] \\
& \times (\mathcal{H}[-y_2]\delta[y_2 + (y_1 + M_\infty c_\infty \tau)\tan\theta] \\
& - \delta[y_2](\mathcal{H}[y_2 + (y_1 + M_\infty c_\infty \tau)\tan\theta] - 1))\delta'[\mathcal{H}[-y_2] \\
& \times (\mathcal{H}[y_2 + (y_1 + M_\infty c_\infty \tau)\tan\theta] - 1) + 1] \\
& \rho v_2 \delta[\mathcal{H}[-y_2](\mathcal{H}[y_2 + (y_1 + M_\infty c_\infty \tau)\tan\theta] - 1) + 1] \\
& \big(cM\mathcal{H}[-y_2]\tan\theta\delta'(\tan\theta(-v_2 + y_1) + y_2) \\
& + M_\infty c_\infty \delta[y_2]\tan\theta\delta[y_2 + (y_1 + M_\infty c_\infty \tau)\tan\theta]\big).
\end{aligned}
\tag{59}
$$

In these four $\mathcal{W}$, p and ρ are the values on the boundary and are part of the boundary condition. Both variables change on the wall. The velocity of the body is based on the ambient condition and the turning angle as

$$
v_1 = -M_\infty c_\infty \text{ m/s and } v_2 = 0 \text{ m/s}. \tag{60}
$$

Based on Eqn. 39, $\mathcal{M}$ is deduced as

$$
\begin{aligned}
\mathcal{M} =& \frac{2M_\infty c_\infty}{p - \rho\,(M_\infty c_\infty)^2} \\
& \times \Big(\rho_\infty + (\rho - \rho_\infty)\mathcal{H}\left[(x_1 + M_\infty c_\infty t)M_\infty^{-1} - x_2(1 - M_\infty^{-1})^{1/2}\right] \\
& \times \mathcal{H}[(x_1 + M_\infty c_\infty t)\sin\theta + x_2\cos\theta]\Big).
\end{aligned}
\tag{61}
$$

Sources $\mathcal{W}_{lm}$ are multiplied with $\mathcal{M}$. These operations result in integrals containing many terms in the integrand. Though integrals involve the same structure as those presented previously and involve combinations of Heaviside, Dirac delta functions, and their derivatives. After analytical integration, the density field is derived and placed in the form using Eqn. 21. The density field of a Prandtl-Meyer expansion at a discrete corner with large turning angle is

$$
\begin{aligned}
\rho(\boldsymbol{x}, t) =& \rho_\infty \prod_{i=1}^{\infty} \frac{\rho_{i+1}}{\rho_i}\mathcal{H}\left[(x_1 + M_\infty c_\infty t)\sin\mu_i - x_2\cos\mu_i\right] \\
& \times \mathcal{H}\left[(x_1 + M_\infty c_\infty t)\sin\theta + x_2\cos\theta\right].
\end{aligned}
\tag{62}
$$

For evaluation in the Integral Method program, μ_i at i is written

$$\mu_i = \sin^{-1}\left[\frac{1}{M_\infty + (i-1)(M - M_\infty)n^{-1}}\right], \tag{63}$$

where n is the number of interactions evaluated. Equation 62 can be written only with wall M via the auxiliary equation for the ratio of densities with respect to M in an isentropic flow-field as

$$\frac{\rho_{i+1}}{\rho_i} = \left(\frac{2 + M_i^2(\gamma - 1)}{2 + M_{i+1}^2(\gamma - 1)}\right)^{\frac{1}{\gamma - 1}}. \tag{64}$$

Figure 10 shows a series of predicted contours of density from Prandtl-Meyer expansion fans using Eqn. 62. The sub-figures are presented in terms of increasing M_∞ and decreasing θ. Approximately seven contour levels are shown per contour plot. Figure 10b corresponds to $M_\infty = 1$, $\theta = 45$ deg., and $v_1 \approx -343.114$ m/s. Resultant values are $M_2 \approx 2.76445$ and $\rho_2 \approx 0.186977$ kg/m^3. Figure 10b corresponds to $M_\infty = 3/2$, $\theta = 90$ deg., and $v_1 \approx -514.671$ m/s. Resultant values are $M_2 \approx 9.850723$ and $\rho_2 \approx 0.00162151$ kg/m^3. Figure 10c corresponds to $M_\infty = 2$, $\theta = 15$ deg., and $v_1 \approx -686.229$ m/s. Resultant values are $M_2 \approx 2.59845$ and $\rho_2 \approx 0.618445$ kg/m^3. Finally, Fig. 10d corresponds to $M_\infty = 5$, $\theta = 5$ deg., and $v_1 \approx -1715.57$ m/s. Resultant values are $M_2 \approx 5.58562$ and $\rho_2 \approx 0.753395$ kg/m^3. These contours are produced with Mathematica version 13.3. Note that the interior of the wall or region 2 is set at $\rho = \infty$ due to limitations of Mathematica.

Recall that using the present technique of generalized functions to represent f and $\mathcal{M}$ result in multi-valued solutions. If the number of products is large, then the solutions will naturally become smoother and in the limit become continuous. On digital computers used to construct analytical solutions, only a finite number of products can be evaluated. The same solution for an ambient $M_\infty = 5/4$ and $\theta = 5$ degree Prandtl-Meyer expansion fan has been constructed to illustrate the problem. Figure 11 shows two plots of density variation with streamwise position, x_1, at $x_2 = 1$ m. In Fig. 11a, eleven products have been evaluated, and in Fig. 11b, 1,001 products have been evaluated. Evaluations are performed with the IMP code. It is clear that multiple Heaviside functions result in a step like behaviour are present in the lower product evaluation. A very smooth line is apparent in the higher product evaluation. However, the multi-valued solution still exists. For engineering calculations, it is practical to use a balance between the number of product evaluations and averaging the value between each step. All numerical evaluations of analytical solutions in this paper use 1001 products per expansion wave or interaction.

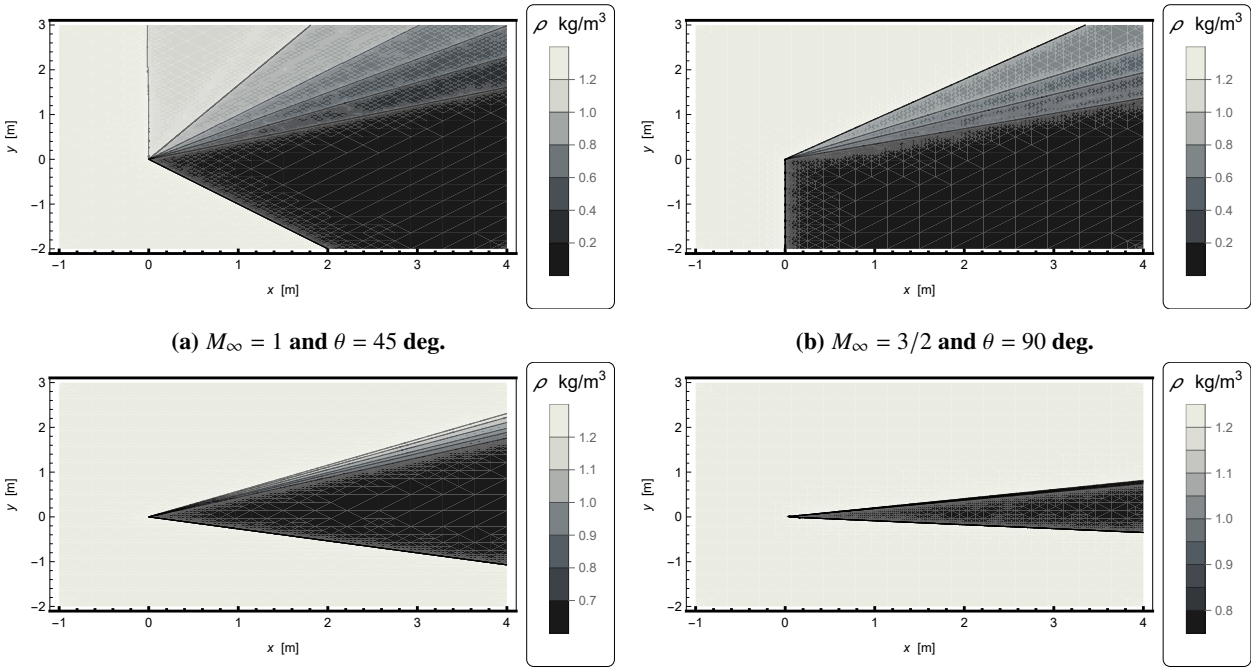

(a) $M_\infty = 1$ **and** $\theta = 45$ **deg.**

(b) $M_\infty = 3/2$ **and** $\theta = 90$ **deg.**

(c) $M_\infty = 2$ **and** $\theta = 15$ **deg.**

(d) $M_\infty = 5$ **and** $\theta = 5$ **deg.**

Fig. 10 Contours of density from Prandtl-Meyer expansion fans.

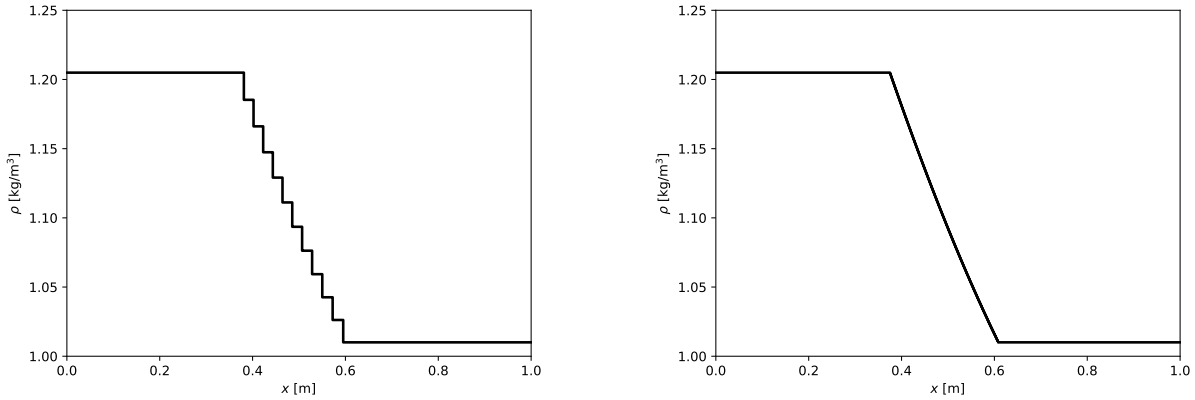

(a) Eleven interactions.

(b) 1001 interactions.

Fig. 11 Density variation within fan in streamwise direction.

D. Prandtl-Meyer Expansion - Single Mach Wave

In the traditional derivation of Prandtl and Meyer [51], only a single Mach wave is considered before its integration to find the solution over the fan. The previous section showed the derivation of the entire wave over a finite angle. To recover the single Mach wave solution, eliminate the product, examine a single change in density, and assume a small turning angle, θ. By using the same functions for the Prandtl-Meyer expansion, f and $\mathcal{M}$, the equation for ρ can be found, which results in a single Mach wave. For $M_1 = 1$, $M_2 = M_1 + \epsilon$, and the small angle approximation for θ, it is found

$$\begin{aligned}\rho(\boldsymbol{x}, t) = &\left(\frac{(\gamma-1)+2}{(1+\epsilon)^2(\gamma-1)+2}\right)^{\frac{1}{\gamma-1}} \\ &\times \mathcal{H}\left[x_1 + c_\infty t\right] \mathcal{H}\left[(x_1 + c_\infty t)\theta_\epsilon + x_2\right] \rho_\infty,\end{aligned} \tag{65}$$

where θ_ϵ indicates a small angle in $\theta \approx \epsilon$ and ϵ is a small real positive number. Equation 65 results in a very small decrease in density in the first quadrant and a Mach wave radiating at 90 deg. moving at velocity v_1, as expected. The first term is the isentropic density ratio across a Mach wave.

E. Wedge-Wall-Flare - No Interaction

A more complex case will now be illustrated to shown construction of a solution that contains no wave interactions. The cone-cylinder-flare is often studied experimentally and numerically, here the corresponding two-dimensional case is examined. The two-dimensional case contains no interactions unlike the three-dimensional case because in inviscid flow the properties on each segment of the aerodynamic body are constant. Thus, to illustrate the approach, a two-dimensional geometry will be used. This is the wedge-wall-flare geometry, and it is illustrated in Fig. 12. The leading edge is located at the origin, $x = y = 0$ m at time $\tau = 0$ s. The first turning angle, $\theta_1 = 5$ deg., is at the origin. At position $y_1 = 1/3$ and $y_2 \approx 0.029163$ m, the wall segment resides at an angle of 1 deg. relative to the y_1-axis and turns the flow by $\theta_2 = -4$ deg., which creates an expansion. A third wall segment is placed at $y_1 = 2/3$ and $y_2 \approx 0.034980$ m, with a local wall turning angle of $\theta_3 = 5$ deg., and the wall segment is at 6 deg. relative to the y_1-axis. The body terminates at $y_1 = 1$ and $y_2 \approx 0.070016$ m. This results in a chord of one meter.

One might be tempted to define f and seek a new unique $\mathcal{M}$, however, the solution can be constructed very easily via products, and in a simpler fashion than the general product Eqn. 21. As previously mentioned, solutions are derived via products, much like linear solutions are found by superposition.

In the near-field, the shock wave, Prandtl-Meyer expansion, and the next shock wave do not interact. The closed-form solution can be written using the previously developed solutions as products (see Eqns. 52 and 62). The equations are off-set by their respective translation in y_1 and y_2 and rotated by their respective θ_2 and θ_3 for the expansion and shock

wave, respectively. Their velocity $\boldsymbol{v}$, remains the same as the leading shock wave.

To illustrate the solution, examine a flow-field with $M_\infty = 1.50$ and standard conditions. The velocity components of the body are $v_1 = -M_\infty c_\infty = 514.67$ m/s and $v_2 = 0$ m/s. Predictions on $x_2 = 1$ m are shown in Fig. 13. The y-axis represents the normalized quantity, and the x-axis represents the normalized streamwise direction with respect to chord. p and M are also shown as a function of x/c, where c is the chord of unit length. This solution, where products are used to construct the field, breakdown immediately when the first wave interaction occurs. That is specifically when the Prandtl-Meyer fan interacts with the shock wave. The predictions agree with traditional theory (see Shapiro [44]).

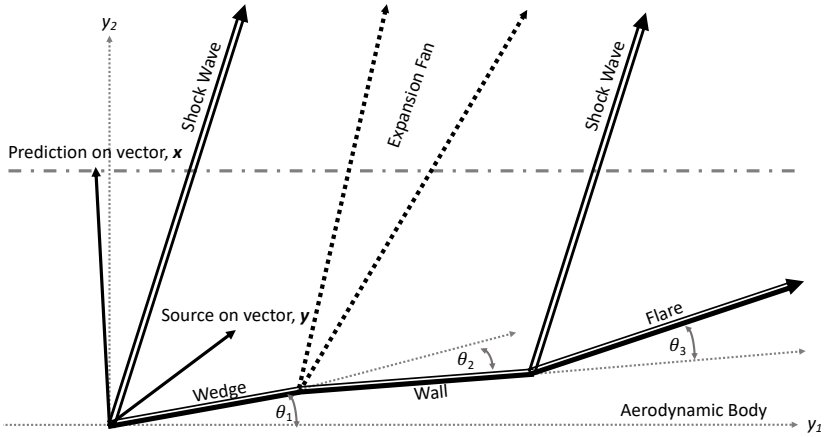

Fig. 12 Diagram of wedge-wall-flare.

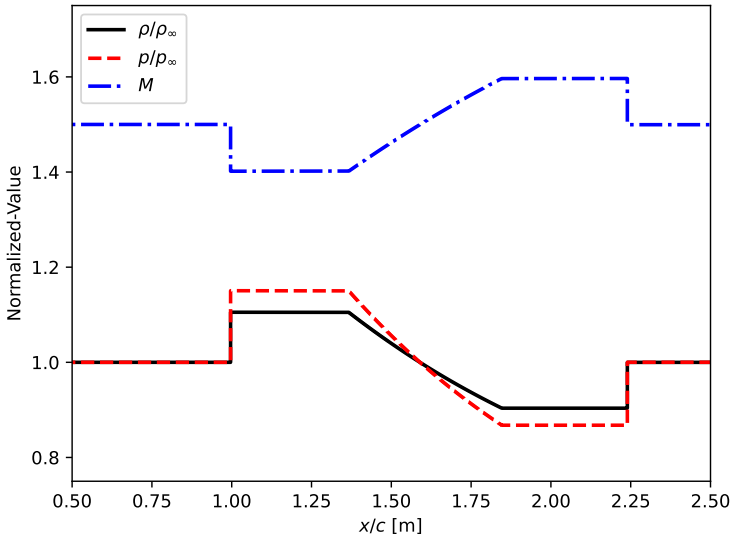

Fig. 13 Normalized density, pressure, and Mach number for the wedge-wall-flare body.

F. Double Wedge - Single Interaction

A double wedge is now examined, where a single interaction occurs between two left-running shock waves. The problem is illustrated in Fig. 14. Initially, the flow is deflected by θ_1 and then a second time by θ_2. This creates two left-running oblique shock waves. They merge and become a single left-running oblique shock wave. The radiated merged shock wave is stronger than the first two. It is clear that there is a single interaction and product solutions must be used via Eqn. 21. The first and second shock waves have individual radiation angles β_1 and β_2, respectively. The total deflection angle of the coalesced shock wave is labeled β_3. All β angles are relative to the incoming flow direction. This notation corresponds to contemporary compressible flow theory (see Anderson [52]).

A single product of solutions is used after applying Eqn. 21 for each individual oblique shock wave. The second shock wave, originating from the surface, is rotated and translated before applying the product. At the intersection location, which can be calculated using simple geometry, another product of solution is applied for region 4. One final product of solutions is used for the region between 4 and the slip line. However, for sonic boom calculations at high-speeds, the slip line has little effect on the sonic boom calculation and is ignored.

Examples are created for the simple double wedge interaction at $M_\infty = 2, 5, 7$, and 9. Corresponding wedge geometries have turning angles $\theta_1 = 5$ and $\theta_2 = 7$ degs. for $M_\infty = 2$, $\theta_1 = 7$ and $\theta_2 = 4$ degs. for $M_\infty = 5$, $\theta_1 = 3$ and $\theta_2 = 3$ degs. for $M_\infty = 7$, and $\theta_1 = 4$ and $\theta_2 = 5$ degs. for $M_\infty = 9$. Predictions exactly match traditional theory [44]. Coalescence of each originating left-running shock wave occurs at an axial and radial coordinate. Four interaction locations occur at $y_1 \approx 1.4582$ m and $y_2 = 1$ m for $M_\infty = 2$, $y_1 \approx 2.9255$ m and $y_2 = 1$ m for $M_\infty = 5$, $y_1 \approx 4.7323$ m and $y_2 = 1$ m for $M_\infty = 7$, and $y_1 \approx 4.3694$ m and $y_2 = 1$ m for $M_\infty = 9$. For each shock wave - shock wave interaction $\rho_2 \approx 1.8834$ kg/m^3, $p_2 \approx 191340.58$ Pa, and $M_2 \approx 1.565$ for $M_\infty = 2$, $\rho_2 \approx 2.7191$ kg/m^3, $p_2 \approx 339430.44$ Pa, and $M_2 \approx 3.900$ for $M_\infty = 5$, $\rho_2 \approx 2.3164$ kg/m^3, $p_2 \approx 261772.16$ Pa, and $M_2 \approx 5.931$ for $M_\infty = 7$, and $\rho_2 \approx 3.4878$ kg/m^3, $p_2 \approx 534055.86$ Pa, and $M_2 \approx 6.498$ for $M_\infty = 9$. These predictions correspond with traditional theory as expected.

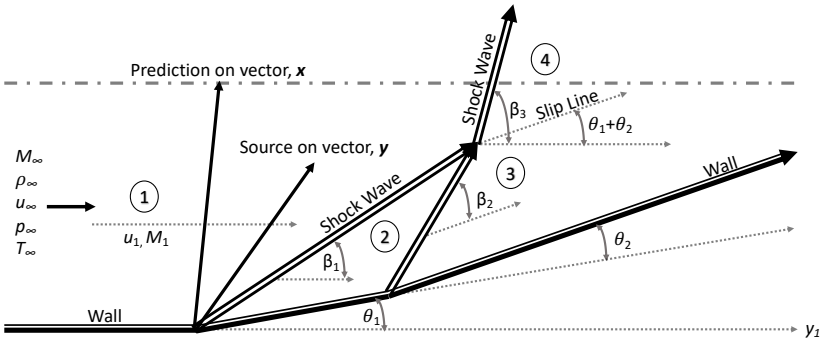

Fig. 14 Diagram of a double oblique shock wave.

G. Diamond Airfoil - Infinite Interactions

The classic diamond airfoil is examined. Unlike the previous double wedge case, this flow-field results in infinite interactions. Interactions occur between the Prandtl-Meyer expansion fan with the leading and trailing shock waves. Figure 15 shows a diagram of the flow-field, which contains leading and trailing shock waves and an expansion fan. The product of Eqn. 21 is evaluated from $i = 1$ to 1001. The leading and trailing edge of the diamond airfoil have local defection angles of $\theta = 5$ deg. The chord of the body is one meter. At half the chord, the turning angle of the expansion is $\theta = -10$ deg. Thickness ratio of the diamond airfoil is $\tau_r \approx 0.04374$. The ambient Mach number $M_\infty = 5$, and all other ambient properties remain those of previous examples.

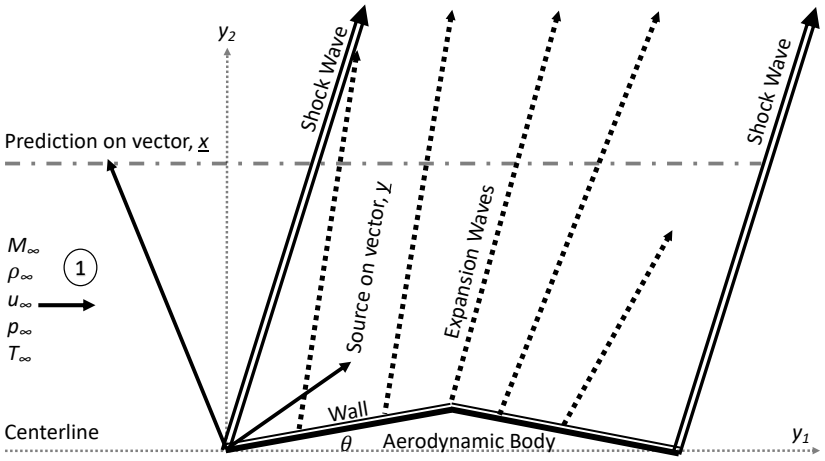

Fig. 15 Diagram of a diamond airfoil aerodynamic body.

Figure 16 shows normalized ρ, p, and M for the diamond airfoil geometry. The y-axis of each sub-figure represents the change in density normalized by ambient density $\Delta\rho\rho_\infty^{-1}$, the change in static pressure normalized by ambient pressure $\Delta p p_\infty^{-1}$, and the difference in Mach number relative to the ambient Mach number, $M - M_\infty$. This style of plot, particularly for p, is commonly used by the sonic boom community to present the aerodynamic near-field for sonic boom propagation solvers, and thus they are chosen for this analysis.

Figure 16a shows predictions with respect to normalized chord and is located at $x_2/c = 1/10$. Figure 16b is located at $x_2/c = 1$, and Fig. 16c is located at $x_2/c = 10$. These cross-stream locations are selected for specific reasons. At the closest location in Figure 16a, no interactions have occurred between any of the waves, which are the two shock waves and expansion waves. At $x_c/c = 1$, some of the expansion waves have interacted with the leading and trailing shock waves, creating a complete near-field prediction.

A prediction outside of the near-field is shown in Fig. 16c, where a complete N-wave forms. It is evident that significant interactions between the shock waves and expansion waves have occurred, which reduces the shock waves strength and extended the duration of the wave form. A classic N-wave has been recovered. It is straightforward to

generate predictions at large propagation distances. By setting $x/c >> 1$, an elongated N-wave of very low amplitude results (see Fig. 16d).

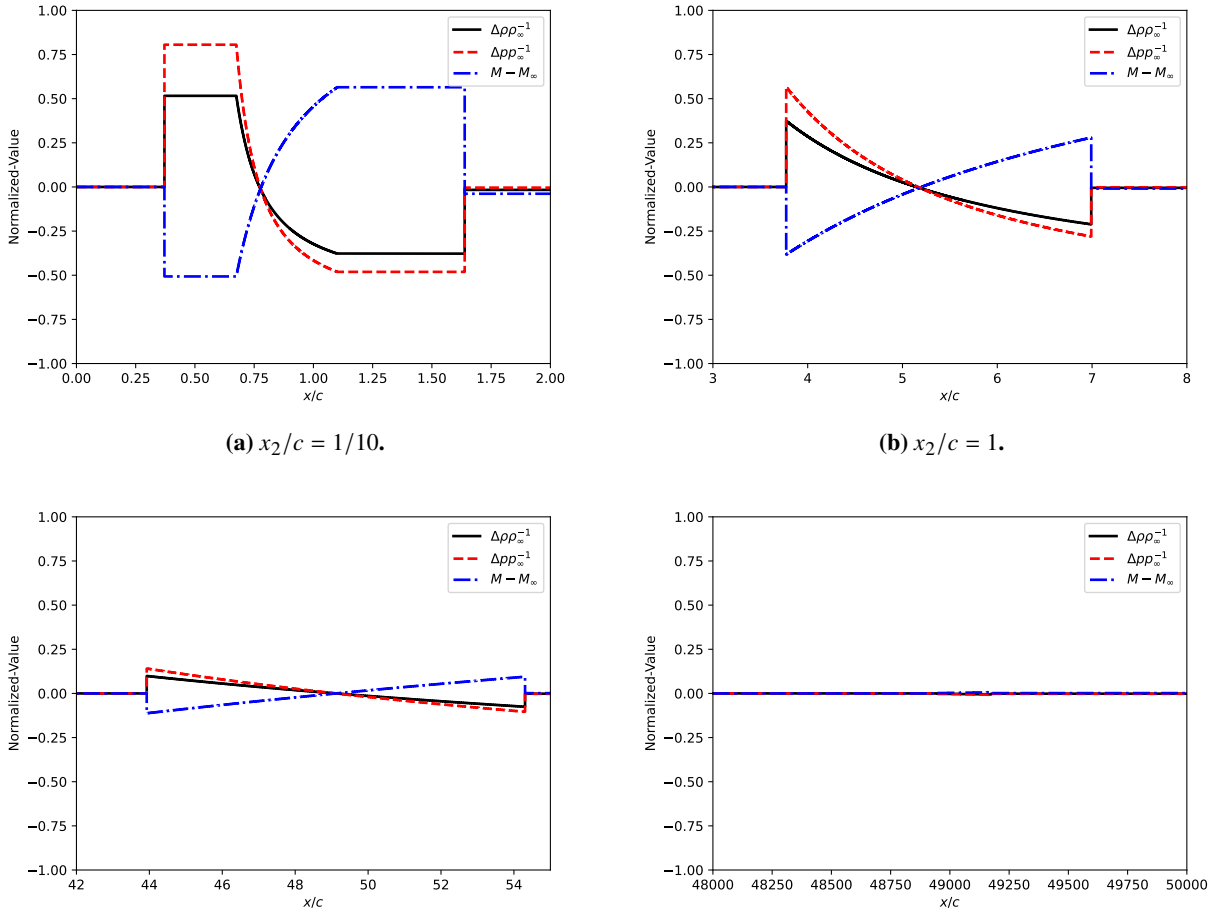

(a) $x_2/c = 1/10$**.**

(b) $x_2/c = 1$**.**

(c) $x_2/c = 10$**.**

(d) $x_2/c = 10,000$**.**

Fig. 16 Normalized density, pressure, and Mach number for the diamond airfoil configuration.

H. A Realistic Test Case: The NASA X-43A

Unfortunately, there are no publicly available published datasets of hypersonic sonic boom from slender waveriders. Nonetheless, an example case will be presented that uses the full method to predict sonic boom from the NASA X-43A. The NASA X-43A project consisted of three flights, two near Mach 7 and one near Mach 10 [53]. The program demonstrated the first Mach 9.70 flight of an airframe-integrated, scramjet-powered, hypersonic vehicle. The third flight of the X-43A, on November 2004, flew at approximately Mach 9.70 at an altitude of 33.36 km. At this particular time of flight, the angle of attack fluctuated considerably between zero and one degree. Booster angle from flight data was reported at 0.08 deg., and the flight-path elevation angle was reported as 1.69 deg.

There is no publicly available geometry of the X-43A, but it has been reconstructed based on multiple descriptions

(see Harsha et al. [54], Navó and Bergada [55]). Prediction of sonic boom from the NASA X43-A is challenging, but represents a good test case of the full method presented here. In particular, since the X-43A is relatively flat on the pressure side and relatively wide, the flow-field on the under-track is relatively more two-dimensional compared to axisymmetric bodies. Thus, the present method is most applicable in the near-field ground track, and a sonic boom propagation solver can predict the signal on the ground through a complicated atmosphere. Unfortunately, exact exhaust data and flow-field information is not available to the public. Thus, Landau's law is applied to the near-field data after the initial shock and expansions waves to predict the remaining waveform that is altered by the exhaust. Off-track predictions are not possible without extension of the present methodology to handle complicated three-dimensional effects.

For the prediction of sonic boom, the altitude is set at 33.36 km, $M_\infty = 9.50$, flight-vehicle length $L \approx 3.6576$ m (from leading edge to trailing fuselage), thickness ratio of 0.06079, $\alpha = 0$ deg., and flight-path elevation angle of 1.69 deg. (see Harsha et al. [54]). The ground reflection factor is 1.90. Propagation is performed with both PCBOOM (see Plotkin et al. [48], Lonzaga [56]) and an updated and integrated waveform parameter method based on Thomas [47]. Due to the high-altitude, the US/NASA atmospheric model [57, 58] is used, which is valid up to 1,000 km.

A slender waverider nearly at Mach 10 in the near-field produces significant over-pressures, however, due to its high altitude the ground signature is very small. At altitude, $p_\infty \approx 728$ Pa. A density ratio rise of approximately 16.51 and $\Delta p/p \approx 0.35988$ across the leading shock wave under the leading edge on the under-track is predicted. Predictions indicate that without thermo-viscous effects in the atmosphere that the waveform will be an N-wave with leading over-pressure of $\Delta p/p_\infty \approx 0.000039$ and trailing pressure recovery to atmospheric of $\Delta p/p_\infty \approx -0.000231$. Duration of the N-wave is predicted as 0.1833 s. At altitude the signal is very quiet and will be considerably altered by atmospheric thermo-viscous effects [59] and atmospheric turbulence [60]. However, if the flight-vehicle were a waverider at a low altitude of 2 km (just above the turbulent boundary layer of the Earth) carrying a kinetic or nuclear weapon, the signal would be much more pronounced and not be an N-wave. If such signals can be detected and compared with the present approach, they can be used for analysis and defense.

IV. Limitations and Future Research

Constructing a combined source function for integration that yields a correct analytical solution, satisfying the Navier-Stokes equations, energy equation, and gas law is extremely challenging. This difficulty cannot be understated. Some new specific solutions have been created via evaluating Eqn. 21. The approach requires a considerable amount of time to ascertain solutions and confirm their validity via the original equations and comparison with traditional approaches, numerics, or experiments. This has been automated to a degree with the new IMP code. However, the method opens a new pathway for finding analytical solutions of interest to the community.

The method, as currently described, is capable of handling viscous effects and higher spatial dimensions in principle,

however, finding $\mathcal{M}$ functions for three-dimensional interactions is difficult. The aerodynamic problem is reduced to finding $\mathcal{M}$ functions. Their existence for many flow-field interactions is unknown. Thus far, predictions have only been demonstrated in one- and two space-time dimensions. Certainly, simple three-dimensional flow-fields can be constructed. However, more complex ones will present significant challenges for researchers and those making predictions for engineering purposes. Also, the number and type of interactions greatly increase in three spatial dimensions for steady flows, and becomes even greater for temporally dependent flow-fields.

The present method is restricted to flow-fields that are entirely supersonic (hyperbolic). In previous numerical parabolized approaches, elliptic methodologies have been utilized in local regions. These methods are numerical and iterative, and could be combined with the present method to create an estimate of flow-fields with greater complexity. An example is the bow shock wave, but the scheme results in a combined analytical-numerical method. The method could be extended in a creative way to predict subsonic flow-fields, and might appear more like Oseen's equation. An extremely creative idea, that does not use past approaches, including the present, must be created to overcome the restriction of hyperbolic flow.

As previously noted for the diamond airfoil case, constructed solutions can be large in size. The diamond airfoil is a two-dimensional solution in time. The total file size of the text file containing the analytical solution is over 300 MB. For three-dimensional cases that are unsteady, the file size could be even larger. However, it does contain in a text format the combination of functions that represent the analytical solution. These solutions can only be interpreted by plotting them through a traditional approach. Plots in this paper were made with a combination of Python and Mathematica whose primary purpose is evaluating and plotting the analytical solution, which was generated by the IMP.

Presently, the method is being extended to handle jet flows with shock waves that radiate from axisymmetric and rectangular nozzles. Also, the predictions for cones and simple axisymmetric aerodynamic bodies with combined sonic boom predictions are in preparation.

V. Conclusion

A new prediction method is devised for finding analytical solutions via direct space-time integration of a combined source-propagation function. The methodology shows promise because the analytical solutions match traditional solutions. Solutions derived in the present paper include the compression wall, the expansion wall, the oblique shock wave, the Prandtl-Meyer expansion wave, a non-interacting wedge-wall-flare, a single interaction oblique shock wave, and the infinite interaction diamond airfoil. One applied prediction is presented to illustrate its use. Unlike traditional theory, all solutions are time-dependent and consist of generalized functions. Hopefully the present methodology can be adapted by the community to explore new two- and three-dimensional high-speed analytical solutions of the Navier-Stokes equations in the aerodynamic near-field.

Acknowledgments

Research was sponsored by the Defense Advanced Research Project Agency (DARPA) and the Army Research Office and was accomplished under Grant Number W911NF-21-1-0342. The views and conclusions contained in this document are those of the authors and should not be interpreted as representing the official policies, either expressed or implied, of the Army Research Office or the U.S. Government. The U.S. Government is authorized to reproduce and distribute reprints for Government purposes notwithstanding any copyright notation herein.

References

[1] Jiang, Z., and Yu, H., "Theories and technologies for duplicating hypersonic flight conditions for ground testing," *National Science Review*, Vol. 4, No. 3, 2017, pp. 290–296.

[2] Bertin, J. J., and Cummings, R. M., "Critical Hypersonic Aerothermodynamic Phenomena," *Annual Review Fluid Mech.*, Vol. 21, No. 38, 2006, pp. 129–157.

[3] Shapiro, A. H., "The Dynamics and Thermodynamics of Compressible Fluid Flow. Vol 2," *New York: Ronald Press*, 1953.

[4] Cheung, S. H., Edwards, T. A., and Lawrence, S. L., "Application of Computational Fluid Dynamics to Sonic Boom Near- and Mid-Field Prediction," *Journal of Aircraft*, Vol. 29, No. 5, 1992, pp. 920–926.

[5] Haering, E., Murray, J., Purifoy, D., Graham, D., Meredith, K., Ashburn, C., and Stucky, M., "Airborne Shaped Sonic Boom Demonstration Pressure Measurements with Computational Fluid Dynamics Comparisons," *43rd AIAA Aerospace Sciences Meeting and Exhibit*, 2005.

[6] Luquet, D., Marchiano, R., Coulouvrat, F., Din, I. S. E., and Loseille, A., "Sonic Boom Assessment of a Hypersonic Transport Vehicle with Advanced Numerical Methods," *21st AIAA/CEAS Aeroacoustics Conference*, AIAA Paper 2015-2685, 2015.

[7] Carpenter, F. L., and Cizmas, P., "UNS3D Simulations for the Third Sonic Boom Prediction Workshop Part II: C608 Low-Boom Flight Demonstrator," *AIAA Aviation 2020 Forum*, American Institute of Aeronautics and Astronautics, 2020.

[8] Whitham, G. B., "The Flow Pattern of a Supersonic Projectile," *Communications on Pure and Applied Mathematics*, Vol. 5, No. 3, 1952, pp. 301–348.

[9] Whitham, G. B., "On the Propagation of Weak Shock Waves," *Journal of Fluid Mechanics*, Vol. 1, No. 3, 1956, pp. 290–318.

[10] Carlson, H., *Correlation of Sonic-Boom Theory with Wind-tunnel and Flight Measurements*, NASA-TR-R-213, 1964.

[11] Hayes, W. D., "Linearized Supersonic Flow," Ph.D. thesis, California Institute of Technology, 1947. Reprinted as North American Aviation Report AL-222: Princeton University AMs Report 852.

[12] Hayes, W. D., and Runyan, H. L., "Sonic-Boom Propagation through a Stratified Atmosphere," *The Journal of the Acoustical Society of America*, Vol. 51, No. 2C, 1972, pp. 695–701. doi:10.1121/1.1912903.

[13] Seebass, A. R., "Hypersonic Boom," *Boeing Scientific Research Laboratories Technical Communication, Vol. 30*, 1970.

[14] Tiegerman, B., "Sonic Booms of Drag Dominated Hypersonic Vehicles," *Ph.D. Dissertation, Cornell University*, 1975.

[15] Plotkin, K., "Review of Sonic Boom Theory," *12th Aeroacoustic Conference, AIAA Paper 1989-1105*, 1989.

[16] Salvetti, A., and Seidman, H., "Noise and Sonic Boom Impact Technology. PCBOOM Computer Program for Sonic Boom Research. Vol. 2. Program Users/Computer Operations Manual." *BBN LABS INC CANOGA PARK CA*, 1988.

[17] Slotnick, J. P., Khodadoust, A., Alonso, J., Darmofal, D., Gropp, W., Lurie, E., and Mavriplis, D. J., "CFD vision 2030 study: a path to revolutionary computational aerosciences," Tech. rep., NASA NTRS, 2014.

[18] Kochkov, D., Smith, J. A., Alieva, A., Wang, Q., Brenner, M. P., and Hoyer, S., "Machine learning–accelerated computational fluid dynamics," *Proceedings of the National Academy of Sciences*, Vol. 118, No. 21, 2021, p. e2101784118.

[19] Cant, S., "High-performance computing in computational fluid dynamics: progress and challenges," *Philosophical Transactions of the Royal Society of London. Series A: Mathematical, Physical and Engineering Sciences*, Vol. 360, No. 1795, 2002, pp. 1211–1225.

[20] Fefferman, C. L., "Existence and smoothness of the Navier-Stokes equation," *The millennium prize problems*, Vol. 57, 2000, p. 67.

[21] d'Alembert, J. L. R., *Traité de l'équilibre et du Mouvement des Fluides: Pour servir de suite au Traité de Dynamique [Treatise on Equilibrium and the Movement of Fluids: To serve as a sequel to the Treatise on Dynamics]*, Paris: David l'ainé, 1744.

[22] Euler, L., "Principes Généraux du Mouvement des Fluides [General Principles of Fluid Movement]," *Mémoires de l'académie des sciences de Berlin*, 1757, pp. 274–315.

[23] Navier, C. L. M. H., "Sur les lois de l'équilibre et du Mouvement des corps élastiques [On the laws of balance and movement of elastic bodies]," *Mem. Acad. R. Sci. Inst. France*, Vol. 6, No. 369, 1827.

[24] Stokes, G. G., "On the Effect of the Internal Friction of Fluids on the Motion of Pendulums," *Transactions of the Cambridge Philosophical Society*, Vol. 9, 1850, p. 8. Read December 9, 1850. Reprinted in Mathematical and Physical Papers, Sir George Gabriel Stokes and Sir J. Larmor, Vol. 3, 1880-1905.

[25] Carlson, H., "Simplified Sonic Boom Prediction," *NASA Technical Paper 1122*, 1978.

[26] Hayes, W. D., "Linearized Supersonic Flow," *Ph.D. Dissertation, California Institute of Technology*, 1947. doi:10.7907/D7N0-4412.

[27] Hayes, W. D., Haefeli, R. C., and Kulsrud, H. E., "Sonic Boom Propagation in a Stratified Atmosphere, with Computer Program," Tech. Rep. CR-1299, NASA, 1969.

[28] Cramer, M. S., "The Problems that Arise in the Generation and Propagation of Sonic Booms: 1. Flow Fields in the Plane of Symmetry Below a Delta Wing; 2. Focusing of an Acoustic Pulse at an Arete," *Ph.D. Dissertation, Cornell University*, 1976.

[29] Cramer, M. S., "Two Problems that Arise in the Generation and Propagation of Sonic Booms: Flow Field in the Plane of Symmetry Below a Delta Wing; and Focusing of an Acoustic Pulse in an Arete," Ph.D. thesis, Cornell University, 1977.

[30] Morris, O., Lamb, M., and Carlson, H. W., "Sonic-Boom Characteristics in the Extreme Near Field of a Complex Airplane Model at Mach Numbers of 1.5, 1.8, and 2," Tech. Rep. TN D-5755, NASA, April 1970.

[31] Hunton, L. W., "Current Research in Sonic Boom," *NASA SP-180*, 1968, pp. 57–66.

[32] Oseen, C. W., "Sur les formules de Green généralisées qui se présentent dans l'Hydrodynamique et sur Quelques-unes de leurs Applications [On the formulas of Green generalisees which are present in hydrodynamics and on some of their applications]," *Acta Mathematica*, Vol. 34, No. 1, 1911, pp. 205–284.

[33] Leray, J., "Sur le Mouvement d'un Liquide Visqueux Emplissant L'Espace [Sur le mouvement d'un liquide visqueux emplissant l'espace]," *Acta Mathematica*, Vol. 63, 1934, pp. 193–248.

[34] Lighthill, M. J., "On Sound Generated Aerodynamically I. General Theory," *Proceedings of the Royal Society of London. Series A. Mathematical and Physical Sciences*, Vol. 211, No. 1107, 1952, pp. 564–587.

[35] Lighthill, M. J., "On Sound Generated Aerodynamically II. Turbulence as a Source of Sound," *Proceedings of the Royal Society of London. Series A. Mathematical and Physical Sciences*, Vol. 222, No. 1148, 1954, pp. 1–32.

[36] Miller, S. A. E., "Toward a Nonlinear Acoustic Analogy: Turbulence as a Source of Sound and Nonlinear Propagation," Tech. Rep. TM-2015-218706, NASA, 2015.

[37] Navier, C. L. M. H., *Mémoire sur les lois de l'équilibre et du Mouvement des corps Solides élastiques [Memory on the laws of balance and movement of elastic solid bodies]*, 1827.

[38] Ffowcs Williams, J. E., and Hawkings, D. L., "Sound Generation by Turbulence and Surfaces in Arbitrary Motion," *Philosophical Transactions of the Royal Society of London. Series A, Mathematical and Physical Sciences*, Vol. 264, No. 1151, 1969, pp. 321–342.

[39] Miller, S. A. E., "Theoretical Aeroacoustics: Compiled Mathematical Derivations of Fereidoun 'Feri' Farassat," Tech. Rep. TM 2016-219179, NASA, 2016.

[40] Weatherburn, C. E., *Differential Geometry of Three Dimensions*, Cambridge University Press, 1927.

[41] Weatherburn, G. E., *An Introduction to Riemannian Geometry and the Tensor Calculus*, Cambridge University Press, 1950.

[42] Gelfand, I. M., and Shilov, G. E., *Generalized Functions*, Vol. 1, Academic Press, London, 1964.

[43] Duffy, D. G., *Green's Functions with Applications*, 1st ed., Chapman and Hall/CRC, 2001.

[44] Shapiro, A. H., "The Dynamics and Thermodynamics of Compressible Fluid Flow. Vol 1," *New York: Ronald Press*, 1953.

[45] Hugoniot, P. H., "Mémoire sur la Propagation du Movement dans les corps et plus Spécialement dans les gaz Parfaits, 1^{e} Partie [Memory on the propagation of movement in bodies and more especially in ideal gases, part 1]," *J. École Polytech. (Paris)*, Vol. 57, 1887, pp. 3–97.

[46] Hugoniot, P. H., "Mémoire sur la Propagation du Movement dans les corps et plus Spécialement dans les gaz Parfaits, 2^{e} Partie [Memory on the Propagation of Movement in bodies and more Specially in Ideal Gases, 2^{e} Part]," *J. École Polytech. (Paris)*, Vol. 58, 1889, pp. 1–125.

[47] Thomas, C. L., "Extrapolation of Sonic Boom Pressure Signatures by the Waveform Parameter Method," *NASA TN D-6832*, 1972.

[48] Plotkin, K. J., Downing, M., and Page, J., "USAF Single Event Sonic Boom Prediction Model: PCBOOM," *The Journal of the Acoustical Society of America*, Vol. 95, No. 5, 1994, pp. 2839–2839.

[49] Reid, J., "The new features of Fortran 2018," *ACM SIGPLAN Fortran forum*, Vol. 37, ACM New York, NY, USA, 2018, pp. 5–43.

[50] Carlisle, D., "OpenMath, MathML, and XSL," *ACM SIGSAM Bulletin*, Vol. 34, No. 2, 2000, pp. 6–11.

[51] Meyer, T., "Über Zweidimensionale Bewegungsvorgänge in einem Gas, das mit Überschallgeschwindigkeit strömt [About two-dimensional movement processes in one Gas flowing at supersonic speeds]," Ph.D. Dissertation, Göttingen University, 1908.

[52] Anderson, J. D., *Hypersonic and High-Temperature Gas Dynamics, 3rd Edition*, American Institute of Aeronautics and Astronautics, Inc., 2019.

[53] Grindle, L., "X-43A Final Flight Observations," *2011 Flight Test Safety Workshop, DFRC-E-DAA-TN3463*, 2011.

[54] Harsha, P., Keel, L., Castrogiovanni, A., and Sherrill, R., "X-43A Vehicle Design and Manufacture," *AIAA/CIRA 13th International Space Planes and Hypersonics Systems and Technologies Conference*, American Institute of Aeronautics and Astronautics, Reston, Virigina, 2005.

[55] Navó, À., and Bergada, J. M., "Aerodynamic study of the NASA's X-43A hypersonic aircraft," *Applied Sciences*, Vol. 10, No. 22, 2020, p. 8211.

[56] Lonzaga, J. B., "Recent Enhancements to NASA's PCBoom Sonic Boom Propagation Code," *AIAA Aviation 2019 Forum*, American Institute of Aeronautics and Astronautics, AIAA Paper 2019-3386, 2019.

[57] United States Committee on Extension to the Standard Atmosphere, "US Standard Atmosphere 1976," *NASA-TM-X-74335*, 1976.

[58] Task Group II to COESA, "The 1976 Standard Atmosphere above 86-km Altitude," *NASA SP-398*, 1976.

[59] King, C. B., Miller, S. A., and Shepard, C. T., "Parametric Study of the Hypersonic Near-Field and Sonic Boom from Waveriders using a Fully-Parabolized Approach," *AIAA SciTech 2024 Forum*, 2024.

[60] Carr, A. N., Lonzaga, J. B., and Miller, S. A. E., "Numerical prediction of loudness metrics for N-waves and shaped sonic booms in kinematic turbulence," *The Journal of the Acoustical Society of America*, Vol. 151, No. 6, 2022, pp. 3580–3593.